Nonlinear stability of hypersonic flow over a cone with passive porous walls

Vipin George, Michael; Stephen, S.O.

DOI:
10.1017/jfm.2012.472

J. Fluid Mech. (2012), *vol.* 713, *pp.* 528–563.
doi:10.1017/jfm.2012.472

Nonlinear stability of hypersonic flow over a cone with passive porous walls

Vipin Michael† and Sharon O. Stephen

School of Mathematics, University of Birmingham, Birmingham B15 2TT, UK

(Received 26 April 2012; revised 29 August 2012; accepted 21 September 2012;
first published online 22 October 2012)

This study investigates the nonlinear stability of hypersonic viscous flow over a sharp slender cone with passive porous walls. The attached shock and effect of curvature are taken into account. Asymptotic methods are used for large Reynolds number and large Mach number to examine the viscous modes of instability (first Mack mode), which may be described by a triple-deck structure. A weakly nonlinear stability analysis is carried out allowing an equation for the amplitude of disturbances to be derived. The coefficients of the terms in the amplitude equation are evaluated for axisymmetric and non-axisymmetric disturbances. The stabilizing or destabilizing effect of nonlinearity is found to depend on the cone radius. The presence of porous walls significantly influences the effect of nonlinearity, and results for three types of porous wall (regular, random and mesh microstructure) are compared.

Key words: compressible flows, compressible boundary layers, instability, nonlinear instability, transition to turbulence

1. Introduction

The transition process from laminar to turbulent flow in hypersonic boundary layers is associated with large changes in both heat transfer and skin friction drag. This can have an impact on the lift and drag, stability and control and heat transfer properties of the flight vehicle (Whitehead 1989; Malik 1990). For design purposes of hypersonic vehicles, for instance in thermal protection systems, predicting the location of transition becomes important (Reed *et al.* 1997). Controlling or delaying the transition to maintain laminar flow over much of the flying surface can result in lower drag, lower surface heat flux and higher fuel efficiency (Kimmel 2003). Extensive experimental, numerical and theoretical studies have been carried out to understand the transition process in a hypersonic boundary layer. As a result of these studies, it is now widely accepted that transition to turbulence in hypersonic flows over smooth bodies and with low levels of free-stream turbulence is associated with amplification of the first and/or second Mack modes. The first Mack mode is the high-speed counterpart of Tollmien–Schlichting waves, so is a viscous instability, with modes located close to the boundary. The second Mack mode is an inviscid instability driven by a region of supersonic mean flow relative to the disturbance phase velocity. The second-mode instability has growth rates that exceed that of the first mode for Mach numbers > 4 (on insulated surfaces). These first and second Mack modes

† Email address for correspondence: michaelv@maths.bham.ac.uk

correspond to the unstable perturbations occurring in the low-frequency band and the high-frequency band, respectively. Fedorov & Tumin (2010) identified a slow (S) mode and a fast (F) mode in the discrete spectrum of the stability analysis of high-speed boundary layers. For relatively hot walls the first and second modes are associated with growth of the slow mode, whereas for relatively cold walls the first mode is associated with the slow mode but the second mode can be associated with the fast mode. Experimental findings (Stetson *et al.* 1983; Fedorov *et al.* 2003*a*,*b*) reveal that the first-mode instability occurs in a lower frequency band, 50–100 kHz, while the second mode occurs around 70–150 kHz, and higher in hypersonic boundary layers over a cone.

Several experimental studies have been conducted on conical models at hypersonic speeds (Stetson *et al.* 1983; Kimmel, Demetriades & Donaldson 1996; Lachowicz, Chokani & Wilkinson 1996; Germain & Hornung 1997; Bountin, Shiplyuk & Sidorenko 2000; Schneider 2004). These experiments confirm the results of linear stability theory (Mack 1984), namely existence of multiple unstable regions, and the dominance of higher frequency second-mode instability. In addition to the first- and second-mode disturbances identified by linear stability theory, subsequent stability experiments (reviewed in Stetson 1988) observed disturbance growth at higher frequencies, which were identified to be higher harmonics of the second-mode disturbances. These were not observed until significant second-mode growth had occurred. Stetson (1988) and Kimmel & Kendall (1991) attribute these findings to nonlinear wave propagation. These early experimental studies are reviewed in Stetson & Kimmel (1992). Nonlinear interactions involving the second mode were observed by Kimmel & Kendall (1991), Chokani (1999) and Shiplyuk *et al.* (2003). These investigations were conducted using bispectral analysis which involves statistical analysis of the disturbance spectrum at various downstream locations. Kimmel & Kendall (1991) and Chokani (1999) observed that harmonic resonance was the dominant nonlinear interaction, while Shiplyuk *et al.* (2003) observed that subharmonic resonance was the primary nonlinear interaction. Kimmel & Kendall (1991) and Chokani (1999) measured naturally occurring disturbances while Shiplyuk *et al.* (2003) made measurements using artificial excitation of controlled disturbances. Investigations by Chokani (2005) on natural disturbances in a 'quiet' wind tunnel identified sum and difference interactions of the second Mack mode. These interactions led to the generation of the first and second harmonic of the second Mack mode. Further investigations following Shiplyuk *et al.* (2003) have been reported in Bountin, Shiplyuk & Maslov (2008) and Maslov, Poplavskaya & Bountin (2010). They observed nonlinear interaction of second-mode waves with disturbances whose frequencies lie in the first-mode frequency range.

Further insight into the transition process beyond frequency interactions can be obtained from studies performing direct numerical simulations (DNS) of the complete Navier–Stokes equations. The spatial DNS study of Bestek & Eissler (1996) at Mach 4.8 was able to confirm the existence of multiple Mack modes. The presence of two further types of secondary instabilities, namely oblique breakdown and fundamental (K-type) breakdown, was observed in the simulations of Husmeier & Fasel (2007). These studies matched the experimental conditions of Stetson & Kimmel (1992). The simulations of Koevary *et al.* (2010) and Laible & Fasel (2011) provide further proof of the relevance of these two transition scenarios in hypersonic boundary layers. Evidence of the oblique transition scenario in hypersonic boundary layers was also provided by the simulations of Pruett & Chang (1995) corresponding to the experiments of Stetson *et al.* (1983). The state of the art in DNS studies on hypersonic

boundary layer stability and transition is given in Zhong & Wang (2012). Much of the current knowledge of the physical mechanisms of hypersonic boundary layer stability and transition, including transition control strategies, is reviewed in Fedorov (2011).

Despite these studies, the physical mechanism of nonlinear breakdown of laminar hypersonic boundary layers is still not completely understood. There is still no consensus on the dominant mechanisms for the breakdown in high-speed flows. The second Mack mode is however thought to be dominant in these nonlinear processes and much scientific attention has been devoted to damping this instability.

Recent experiments reported in Fedorov *et al.* (2001, 2003*a*,*b*, 2006) have shown that porous coatings greatly stabilize the second Mack mode of the hypersonic boundary layer on sharp slender cones. The effect of the porous coating is to reduce the growth rates of the second mode to a level where they are comparable with those of the first Mack mode. In addition, the first mode is observed to be slightly destabilized by the presence of the porous coating. Numerical investigations of Wang & Zhong (2009, 2010, 2011*a*,*b*) for Mach 6 flow over a flat plate also showed that different types of porous coatings destabilized mode S in Mack's first-mode region concurrent with second-mode stabilization. This was also observed in the two-dimensional DNS of Egorov, Fedorov & Soudakov (2008).

Nonlinear aspects of hypersonic flow over porous coatings on a sharp cone are reported in Chokani *et al.* (2005) and Bountin *et al.* (2010) who investigated the nonlinear interaction of artificially excited second-mode disturbances using bispectral analysis. On a solid surface, disturbance amplitude spectra revealed that the second-mode amplitude increased downstream and was always larger than the amplitude of the first mode at a given station. On the porous surface, the amplitude of the second mode was much smaller at all stations and showed only a small change in its amplitude in the downstream direction. However, in contrast to the solid surface, at a particular location on the porous surface, the amplitude of the first mode was larger than that of the second mode. Bispectral measurements show that subharmonic and harmonic resonance of the second mode are observed on the solid surface and are significantly modified on the porous surface. Harmonic resonance which is dominant on the solid surface was completely absent on the porous surface. These studies also observed subharmonic resonance of the first mode on porous surfaces that was not present on the solid surface. Nonlinear interaction between vortex (first-mode) waves and filling of the low-frequency vortex-mode spectrum in the presence of porous walls have also been found by the theoretical analysis of Gaponov & Terekhova (2009). They used a nonlinear interaction model in three-wave resonance systems for compressible flat-plate boundary layers. Gaponov *et al.* (2010) investigated experimentally and theoretically the influence of porous coatings on the stability and transition of a supersonic (Mach 2) boundary layer over a flat plate. They found that the use of a porous coating destabilizes the disturbances in supersonic boundary layers (oblique first-mode type) and accelerates boundary-layer transition. Transition of a Mach 6 boundary layer over a flat plate with porous coating was also investigated by three-dimensional temporal DNS of De Tullio & Sandham (2010). Their calculations revealed that an oblique first-mode wave is the most amplified mode in the presence of the porous surface. This wave is slightly destabilized by the porous coating. With the oblique first mode excited, the flow becomes turbulent due to nonlinear interactions without the need for secondary instabilities (as is the case over solid surfaces).

In the light of these results, a detailed theoretical investigation of the stability of Mack's first-mode disturbances for flow over a sharp slender cone is undertaken. Three different types of porous walls are modelled using the formulation developed

by Fedorov *et al.* (2003*b*) and Kozlov, Fedorov & Malmuth (2005). These porous-wall models are characterized by an admittance which is a function of the disturbance frequency and depends on the physical properties of the flow and the porous layer. The focus of this paper is the effect of these types of porous walls on the nonlinear stability of the first Mack mode. In this theoretical and asymptotic investigation for large Mach number and large Reynolds number, the scales used are appropriate to the first Mack mode instability which is governed by a triple-deck structure (Neiland 1969; Stewartson & Williams 1969). The effects of curvature and the attached shock are taken into account. Curvature effects are important as the local radius at the point of interest is larger than the boundary-layer thickness. The stability analysis of Duck & Hall (1989, 1990) for supersonic flow over axisymmetric bodies shows that neutral curves bear no resemblance to those in the absence of curvature. Significant differences between the stability of hypersonic planar and conical boundary layers were also elucidated by the experiments of Stetson *et al.* (1991). The influence of an attached shock on the growth rates of Tollmien–Schlichting waves was demonstrated by Cowley & Hall (1990) and Chang, Malik & Hussaini (1990). A significant result is that the presence of a shock gives rise to an infinite number of unstable modes. Numerical studies by Stilla (1994), Stuckert & Reed (1994) and Leung & Emanuel (1995) also conclude that the effect of the shock must be taken into account. The first theoretical investigation taking into account effects of both the shock and curvature was undertaken by Seddougui & Bassom (1997). Their study concluded that when the attached shock is taken into account, the effect of curvature is significant. Modes which exist in the absence of a shock were now totally destroyed. Multiple modes are possible as in the planar case. However, in contrast to the planar case, the influence of shock is always there. Stephen & Michael (2010*a*,*b*) extended the linear stability study of Seddougui & Bassom (1997) by considering the porous wall. Comprehensive accounts of these results in flow regimes relevant to experimental conditions are presented in Michael (2012) and Stephen & Michael (2012), including the effect of the porous-wall parameters on spatial growth rates.

As a first theoretical investigation into the effects of nonlinearity taking into account the attached shock, Stephen (2006) extended the study of Seddougui & Bassom (1997) into the weakly nonlinear regime. The current paper presents the first theoretical investigation into the effect of passive porous walls on the nonlinear stability of Mack's first-mode disturbances that includes the effect of attached shock and curvature. We extend the analysis of Stephen (2006) to include the effects of various porous-wall models and present results in flow regimes relevant to typical experimental conditions. Stephen (2006) used incorrect values to evaluate one of the nonlinear coefficients. This paper presents corrected results for the solid-wall problem and compares them with those obtained considering the porous wall. The plan of the paper is as follows. In § 2 the problem of hypersonic flow over a sharp cone is formulated. The ranges of validity of the subsequent analysis appropriate to viscous modes are stated here. The porous-wall models and triple-deck structure for non-axisymmetric and axisymmetric disturbances are also given here. A weakly nonlinear analysis of the governing equations is presented in § 3. The outcome of the analysis is that an equation for the amplitude of disturbances is obtained. The values of the coefficients in this equation are significant and are evaluated in § 4 with the results being discussed in § 5.

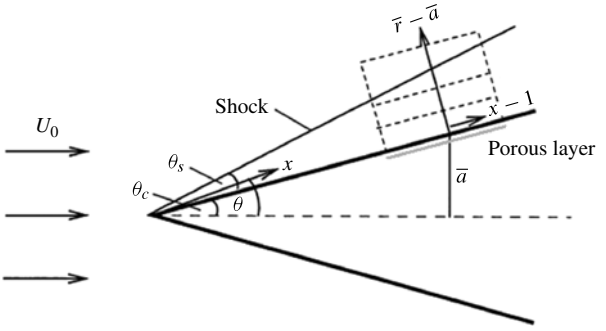

FIGURE 1. Geometry of the cone and shock.

2. Formulation

We will examine the stability of hypersonic flow over a cone with porous walls taking into account the attached shock and curvature. The stability of the basic flow is investigated in a weak interaction region following the triple-deck formulation in § 2.3. Here weak interaction is defined by the parameter $\chi = M_\infty Re^{-1/6} \ll 1$ (Stewartson 1964; Brown *et al.* 1991), where M_∞ and Re are the Mach number and Reynolds number in the free stream respectively. This implies that we are considering a location far enough from the nose of the cone to ensure that viscous–inviscid interaction between the boundary layer and inviscid flow is small (Stewartson 1964).

2.1. *Basic flow*

The flow of a compressible viscous gas over a sharp cone with a porous boundary, of semi-angle θ_c, is considered at hypersonic speed U_0 aligned with the cone axis. The attached shock makes an angle θ_s with the cone surface. The situation is illustrated in figure 1. The dashed lines in this figure indicate the triple-deck structure of the flow, details of which are given in § 2.3. Spherical polar coordinates (x, θ, ϕ) are used to describe the basic flow. Here ϕ denotes the azimuthal angle. The radial distance x has been non-dimensionalized with respect to L^*, the distance from the tip of the cone to the location under consideration. Away from the surface of the cone, viscous effects are neglected and the fluid velocities, pressure and density satisfy the conservation-of-mass, Euler and energy equations. The velocities are non-dimensionalized with respect to U_-, the magnitude of fluid velocity just behind the shock. The time, pressure and density are non-dimensionalized with respect to L^*/U_-, $\rho_- U_-^2$, and ρ_-, respectively, with ρ_- being the density behind the shock. Finally the temperature is non-dimensionalized with respect to T_-, the temperature just behind the shock.

The inviscid axisymmetric flow between the cone surface and the conical shock depends only on the polar angle θ. The jump conditions at the shock must be considered and the velocity components may be obtained from the numerical solution of the Taylor–Maccoll equations (Taylor & Maccoll 1933). A constant-density approximation can be made as a lower-order approximation to the exact Taylor–Maccoll equations in the hypersonic limit ($M_\infty \to \infty$). For slender cones ($\theta_c \to 0$), this approximation agrees well with the exact solution (see Rasmussen 1994, chap. 3.4). This hypersonic small-disturbance approximation to the basic flow

gives an approximate value of the shock angle as

$$\sin\sigma = \sin\theta_c\left(\frac{\gamma+1}{2} + \frac{1}{M_\infty^2\sin^2\theta_c}\right)^{1/2}, \tag{2.1}$$

where $\sigma = \theta_s + \theta_c$ and γ is the specific heat ratio of air. Note that the term $M_\infty \sin\theta_c$ is $O(1)$. Thus, the shock angle may be calculated for a fixed cone angle and free-stream Mach number. A rough indication of the results is that $\theta_s \approx \theta_c$. This is consistent with the ensuing local analysis since we take the thickness of the upper deck (where the shock is located) to be comparable with the radius of the cone (§ 2.3). Thus, the effect of the shock should not be neglected.

So taking the ratio of gas densities just ahead of the shock and just behind to be small we use the steady constant-density solution of Hayes & Probstein (1966) which has the advantage of analytical expressions for the velocity components and pressure. A complete description of the basic flow solution and its validity is given in Seddougui & Bassom (1997) and Michael (2012).

These inviscid solutions are not valid close to the surface of the cone, so we introduce a boundary layer in this region. For our analysis we define the Reynolds number as $Re = \rho_- U_- L^*/\mu_-$ and take it to be large. We take θ_c to be small to correspond to recent experiments. The flow between the shock and cone satisfies the conservation-of-mass, Navier–Stokes and energy equations in terms of non-dimensional coordinates $(x, \bar{r}, \phi)$ and Mach number M, just behind the shock; x and ϕ are as defined previously and $L^*\bar{r}$ is the normal direction to the cone surface where $\bar{r} = \bar{a}$ on the cone generatrix. The corresponding non-dimensional flow velocities, pressure and density are (u, v, w), p and ρ respectively. The non-dimensional temperature and viscosity on the cone surface are respectively denoted by T_w and μ_w. The boundary conditions imposed are no-slip (coupled to the porous layer) at the cone surface and jump conditions at the shock. Following Seddougui & Bassom (1997) the only restriction imposed on the temperature boundary condition is $T_w \gg 1$, which is violated only for situations involving strong cooling on the cone wall. Usually the wall temperature is taken to be $T_w = T_b T_r$, where T_r is the adiabatic wall temperature given by $T_r = 1+\sqrt{Pr}M^2\,(\gamma-1)\,/2$ where Pr is the Prandtl number. Thus unless the constant T_b is very small, T_w will be of $O((\gamma-1)M^2)$ for both adiabatic walls ($T_b = 1$) and isothermal walls. The analysis is unaffected by the particular choice of temperature–viscosity law. The choice only affects the bounds placed on various parameters of the problem. Sutherland's viscosity law ($\mu_w \sim (1+\overline{C})T_w^{1/2}$, $\overline{C}$ being a constant) is used henceforth. The conditions to be satisfied at the shock by a disturbance to the basic flow are derived in detail by Seddougui (1994). Cowley & Hall (1990) showed for the inclined shock over a wedge, with the appropriate scales for the pressure perturbation (as acoustic waves), that the leading-order pressure perturbations were zero at the shock. The corresponding analysis for the cone by Seddougui (1994) shows the same result, although the flow between the shock and the cone is not uniform.

2.2. *Porous boundary*

We will present results corresponding to three different porous surfaces used in previous experimental investigations (Fedorov *et al.* 2003*b*; Maslov 2003; Lukashevich *et al.* 2010). In all cases the porous layer admittance $\overline{A_y}$ can be expressed in the form

$$\overline{A_y} = -(\phi_0/Z_0)\tanh(\Lambda h_0), \tag{2.2}$$

where ϕ_0 is the porosity, h_0 is the non-dimensional thickness and Z_0 and Λ are the characteristic impedance and propagation constant of an isolated pore, respectively. For non-dimensionalization of the porous-layer parameters the reference length is chosen as the boundary-layer displacement thickness δ^* and the reference time scale as δ^*/U_- to be consistent with published studies. In the formulation dimensional quantities are denoted with an asterisk.

Fedorov *et al.* (2006) give the following expressions for the porous-layer characteristics:

$$Z_0 = \frac{\sqrt{\rho_D/C_D}}{M\sqrt{T_w}} \quad \text{and} \quad \Lambda = \frac{\mathrm{i}\omega M}{\sqrt{T_w}}\sqrt{\rho_D C_D}, \tag{2.3}$$

where ω is the frequency of disturbance propagation in the pore. These are functions of the complex dynamic density ρ_D and complex dynamic compressibility C_D. The precise definitions of these quantities depends on the structure of the porous wall and are given below for the cases investigated here. The wall boundary condition, in all cases, is then given by

$$v = \overline{A_y}\,(p - p_-)\,, \tag{2.4}$$

where v and p are the non-dimensional wall-normal velocity component and pressure respectively and $p_- = \gamma^{-1}M^{-2}$.

2.2.1. *Regular microstructure*

Following Fedorov *et al.* (2001, 2006) we consider the porous layer on the cone surface to be a sheet of thickness h^* perforated with cylindrical blind holes of radius r_p^* and equal spacing $s^* = r_p^*\sqrt{\pi/\phi_0}$. This model takes into account gas rarefaction effects. We have

$$\left.\begin{aligned} \rho_D &= \frac{1}{1 - F(B_v, \zeta)}, \quad C_D = 1 + (\gamma - 1)F(B_E, \widetilde{\zeta}), \\ F(B, \zeta) &= \frac{G(\zeta)}{1 - 0.5B\zeta^2 G(\zeta)}, \end{aligned}\right\} \tag{2.5}$$

where

$$B_v = (2\alpha_v^{-1} - 1)Kn, \quad B_E = \left[2\frac{\gamma(2\alpha_E^{-1} - 1)}{(\gamma + 1)Pr}\right]Kn, \quad G(\zeta) = \frac{2\mathrm{J}_1(\zeta)}{\zeta \mathrm{J}_0(\zeta)}, \tag{2.6}$$

with $\zeta = r_p\sqrt{\mathrm{i}\omega\rho_w R/\mu_w}$ and $\widetilde{\zeta} = \zeta Pr$. Here $\mathrm{J}_{0,1}$ are Bessel functions of the first kind, α_v and α_E are molecular accommodation coefficients, Kn is the Knudsen number and R is the Reynolds number based on the boundary-layer displacement thickness of the gas flow.

2.2.2. *Mesh microstructure*

Following Lukashevich *et al.* (2010) we consider the porous coating on the cone surface to comprise several layers of stainless-steel wire mesh of half-pore width $\widetilde{a}^*$ as shown in figure 3 of their paper. A similar model to the one described in § 2.2.1 for a regular microstructure is employed. Following Kozlov *et al.* (2005) we have different expressions for the complex dynamic density and compressibility. Hence we can obtain the following expressions for the porous-layer characteristics for a

square-mesh microstructure:

$$\left.\begin{aligned} &\rho_D = 1/(1 - F(\beta_m, \zeta)), \qquad C_D = 1 + (\gamma - 1)F(\widetilde{\beta_m}, \widetilde{\zeta}), \\ &F(\beta_m, \zeta) = 1 + \zeta^2 \sum_{m=0}^{\infty} \left[\frac{2}{\gamma_m^2 \beta_m^2} \left(1 - \frac{\tanh(\beta_m)}{\beta_m} \right) \right], \end{aligned} \right\} \tag{2.7}$$

where

$$\gamma_m = \pi \left(m + \tfrac{1}{2} \right), \qquad \beta_m = \sqrt{\gamma_m^2 - \zeta^2}, \qquad \widetilde{\beta_m} = \sqrt{\gamma_m^2 - \widetilde{\zeta}^2}, \tag{2.8}$$

with $\zeta = \widetilde{a}\sqrt{\mathrm{i}\omega\rho_w R/\mu_w}$. Following Lukashevich *et al.* (2010) gas rarefaction effects are neglected in this model.

2.2.3. *Random microstructure*

Following Fedorov *et al.* (2003*b*) we consider the porous layer on the cone surface to have a random microstructure of felt metal fibres of diameter d^*. A similar model to the one used for the regular microstructure is employed. We have different expressions for the complex dynamic density and compressibility. Fedorov *et al.* (2003*b*) give the following expressions for the porous-layer characteristics for flow over a felt metal microstructure:

$$\left.\begin{aligned} &\rho_D = a_\infty \left(1 + \frac{g(\lambda_1)}{\lambda_1} \right), \quad C_D = \gamma - \frac{\gamma - 1}{1 + \dfrac{g(\lambda_2)}{\lambda_2}}, \\ &g(\lambda_i) = \sqrt{1 + \frac{4 a_\infty \mu_w^* \lambda_i}{\sigma^* \phi_0 r_p^{*2}}}, \quad \lambda_1 = \frac{\mathrm{i} a_\infty \rho_w^* \omega^*}{\phi_0 \sigma^*}, \quad \lambda_2 = 4Pr\lambda_1, \end{aligned} \right\} \tag{2.9}$$

where the characteristic pore size is calculated as

$$r_p^* = \frac{\pi d^*}{(1 - \phi_0)(2 - \phi_0)}. \tag{2.10}$$

Here μ_w^*, ρ_w^*, and ω^* are dimensional wall viscosity, wall density and frequency respectively and σ^* is the flow resistivity whose value is chosen to fit the experimental data for flow over the felt metal. The tortuosity a_∞ is taken to be unity. Following Fedorov *et al.* (2003*b*) gas rarefaction effects are neglected.

2.3. *Triple-deck structure*

The stability of the basic flow to Tollmien–Schlichting (first-mode) waves for $Re \gg 1$ and $M \gg 1$ is governed by a triple-deck structure. This formulation was used by Cowley & Hall (1990) for flow over a wedge and by Duck & Hall (1989, 1990) for flow over cylindrical bodies. The details of the structure are only summarized here, as it exactly follows the work by Seddougui & Bassom (1997) and Stephen (2006) for flow over a cone with a solid wall. It was shown by Smith (1989) that an asymptotic description of Tollmien–Schlichting waves can be obtained for wave directions sufficiently oblique to lie outside the local wave-Mach-cone direction ($\tan\theta > \sqrt{M_\infty^2 - 1}$), where M_∞ is the free-stream Mach number. In the limit of large Mach number, Smith (1989) derived the frequencies and the x- and ϕ-direction wavelengths of the most rapidly growing waves. These fix the time and length scales of the first-mode disturbances. To adopt the classical triple-deck formulation, we argue that at large Reynolds numbers, the normal direction variation of our disturbances

exhibits three main scales: lower deck which is the viscous sublayer, the main deck which is the main boundary layer and the upper deck containing potential flow. We exclude non-parallel effects by requiring the wavelength of the disturbance to be much less than the distance from the cone apex. Cowley & Hall (1990) showed the required restriction to be $\gamma - 1 \ll 1$, called the 'Newtonian assumption'. Note that here we also have $(\gamma - 1)M^2 \gg 1$. We can study how the growth rates of the oblique first-mode disturbances are modified by the presence of a shock as the shock lies in the upper deck. For a fixed free-stream Mach number and cone angle, as shown earlier, $\theta_s \approx \theta_c$. This makes the thickness of the upper deck (where the shock is located) comparable with the radius of the cone, allowing us to capture the effects of the shock. Pressure disturbances that develop in the lower deck generate a velocity perturbation normal to the cone (and shock) in the upper deck. In order that the linearized shock condition remains applicable we require the undisturbed velocity normal to the shock (from the inviscid flow solution) to be larger than this generated velocity perturbation. Cowley & Hall (1990) have shown that to satisfy all these conditions, we need to impose restrictions on the magnitudes of Mach number M and angle $\sigma = \theta_c + \theta_s$ arising from the inviscid flow solution. The actual scaling is dependent on the choice of viscosity law. For Sutherland's viscosity law we have

$$Re^{1/9} \ll M \ll Re^{7/37}, \quad Re^{-1/9} \ll \sigma \ll Re^{-1/37}. \tag{2.11}$$

For a typical wind tunnel experiment conducted on 0.5 m long 7° half-angle cone models at a free-stream Mach number $M_\infty \approx 6$ and unit Reynolds numbers $Re_1 \approx 10^7$, (2.11) requires that the shock angle σ be bounded as $12.3° < \sigma < 39.4°$ and that the Mach number behind the shock be bounded as $4.64 < M < 13.7$. Recall that $\theta_s \approx \theta_c$, so $\sigma \approx 2\theta_c$. We can thus expect the asymptotic analysis to capture physically realistic hypersonic flow regimes. Equation (2.11) also ensures that the lower-deck problem is nonlinear. If the lower deck is forced to remain linear then the upper bound on σ relaxes to $\sigma \ll Re^{-1/107}$. The lower bound is attained when the non-parallel assumption is violated.

We now restrict our attention to a location along the cone surface where the non-dimensional radius $\bar{a} \sim Re^{-3/8}M^{-1/4}\mu_w^{3/8}T_w^{9/8}$. This restriction ensures that the boundary-layer thickness, $O(Re^{-1/2}L^*)$, is small compared to the cone radius allowing the subsequent analysis to capture the effects of curvature on the stability problem. For smaller values of radius, $\bar{a}$, the problem reduces to that of the planar case (flow over a wedge). The values of $\bar{a}$ will be chosen to correspond to prior studies (see § 4). The angle of the cone and the flow parameters from these studies enable the corresponding value of $\bar{a}$ to be obtained. It is convenient to scale out parameters such as T_w and μ_w as shown by Cowley & Hall (1990) to simplify the analysis. Thus, the following scales are introduced:

$$x = 1 + Re^{-3/8}\mu_w^{3/8}T_w^{9/8}M^{3/4}X, \tag{2.12a}$$

$$\bar{a} = Re^{-3/8}\mu_w^{3/8}T_w^{9/8}M^{-1/4}a, \tag{2.12b}$$

$$t = Re^{-1/4}\mu_w^{1/4}T_w^{3/4}M^{1/2}\tau. \tag{2.12c}$$

These scales are fixed throughout the triple-deck structure.

2.3.1. *Lower deck*

The lower deck is the region in which viscous effects are important. The nonlinearity of the problem appears here. The scalings here take the form

$$\bar{r} - \bar{a} = Re^{-5/8}\mu_w^{5/8}T_w^{7/8}M^{1/4}Y, \tag{2.13a}$$

$$u \sim Re^{-1/8}\mu_w^{1/8}T_w^{3/8}M^{1/4}U, \tag{2.13b}$$

$$v \sim Re^{-3/8}\mu_w^{3/8}T_w^{1/8}M^{-1/4}V, \tag{2.13c}$$

$$w \sim Re^{-1/8}\mu_w^{1/8}T_w^{3/8}M^{-3/4}W, \tag{2.13d}$$

$$\overline{A_y} \sim Re^{-1/8}\mu_w^{1/8}T_w^{3/8}M^{5/4}A_y, \tag{2.13e}$$

$$p \sim \gamma^{-1}M^{-2} + Re^{-1/4}\mu_w^{1/4}T_w^{-1/4}M^{-3/2}P, \tag{2.13f}$$

$$T \sim T_w, \tag{2.13g}$$

$$\rho \sim T_w^{-1}. \tag{2.13h}$$

Substituting these expressions into the non-dimensional continuity and Navier–Stokes equations gives to leading order

$$U_X + V_Y + \frac{1}{a}W_\phi = 0, \tag{2.14a}$$

$$U_\tau + UU_X + VU_Y + \frac{W}{a}U_\phi = U_{YY}, \tag{2.14b}$$

$$W_\tau + UW_X + VW_Y + \frac{W}{a}W_\phi = -\frac{1}{a}P_\phi + W_{YY}. \tag{2.14c}$$

In the hypersonic limit ($M \to \infty$) the term P_X does not appear at leading order. The conditions to be satisfied on the surface of the cone are no-slip (coupled to the porous boundary). In addition, the solution here must match with the main deck in the limit $Y \to \infty$. Thus the necessary boundary conditions to be satisfied are

$$U = W = 0 \quad \text{and} \quad V = A_y P \quad \text{on } Y = 0, \tag{2.15a}$$

$$U \to \lambda(Y + A(X, \phi, \tau)), \quad W \to D/Y \quad \text{as } Y \to \infty. \tag{2.15b}$$

Here A is a displacement function whose evolution will be obtained from the nonlinear stability analysis and D satisfies the equation $D_X = -P_\phi/a$. λ is the boundary-layer skin friction from the undisturbed middle-deck solution.

2.3.2. *Middle deck*

The middle deck has the same thickness as the undisturbed boundary layer. Since $T_w \gg 1$ for $M \gg 1$, there exists a thin transition region in which T is quickly reduced to its free-stream value of unity. Thus the middle deck consists of three regions: (i) a high-temperature boundary-layer region (where $T \sim O(M^2)$) of thickness $O(Re^{-1/2}M^{3/2})$; (ii) a thin region of $O(Re^{-1/2})$ thickness ($T \sim O(1)$); and (iii) a small transition region between the two. Similar solutions occur in all three regions, and we focus on region (i) where the basic temperature is large and find the scalings here to be

$$\bar{r} - \bar{a} = Re^{-1/2}\mu_w^{1/2}T_w^{1/2}y, \tag{2.16a}$$

$$u \sim \overline{U_0(y)} + Re^{-1/8}\mu_w^{1/8}T_w^{3/8}M^{1/4}A\overline{U_{0y}}, \tag{2.16b}$$

$$v \sim Re^{-1/4}\mu_w^{1/4}T_w^{-1/4}M^{-1/2}A_X\overline{U_0}, \tag{2.16c}$$

$$w \sim Re^{-1/4}\mu_w^{1/4}T_w^{-1/4}M^{-1/2}D\overline{U_0R_0}, \tag{2.16d}$$

$$p \sim Re^{-1/4}\mu_w^{1/4}T_w^{-1/4}M^{-3/2}P, \tag{2.16e}$$

$$\rho \sim \overline{R_0(y)} + Re^{-1/8}\mu_w^{1/8}T_w^{3/8}M^{1/4}A\overline{R_{0y}}. \tag{2.16f}$$

Here $\overline{U_0}$ and $\overline{R_0}$ are the non-dimensional velocity and density respectively of the basic boundary-layer flow.

2.3.3. *Upper deck*

In the upper deck the basic flow quantities go to their values just below the shock. It is here that the curvature effects are important. Since the shock location is within the upper deck we require that $\theta_s \sim Re^{3/13}M^{-40/13}$ for Sutherland's law (Stephen 2006). The disturbances here can be scaled as pressure–acoustic waves using

$$\bar{r} = Re^{-3/8}\mu_w^{3/8}T_w^{9/8}M^{-1/4}r, \tag{2.17a}$$

$$p \sim Re^{-1/4}\mu_w^{1/4}T_w^{-1/4}M^{-3/2}\tilde{p}. \tag{2.17b}$$

The governing inviscid equations then reduce after simplification to

$$\frac{\partial^2\tilde{p}}{\partial r^2} + \frac{1}{r}\frac{\partial\tilde{p}}{\partial r} + \frac{1}{r^2}\frac{\partial^2\tilde{p}}{\partial\phi^2} - \frac{\partial^2\tilde{p}}{\partial X^2} = 0. \tag{2.18}$$

The boundary conditions to be satisfied are obtained by matching the solution with the main deck as $r \to a$, and by applying the necessary constraint at the location of the shock ($r = r_s$). The matching condition yields

$$\tilde{p}_r = A_{XX} \quad \text{and} \quad \tilde{p} = P \quad \text{at } r = a. \tag{2.19}$$

By considering linear waves beneath the shock, Seddougui (1994) shows the required shock condition to be

$$\tilde{p} = 0 \quad \text{at } r = r_s. \tag{2.20}$$

As a result of the shock, the solution to (2.18) will allow outgoing and incoming waves (Kluwick, Gittler & Bodonyi 1984).

2.4. *Axisymmetric problem*

We now discuss the solution for axisymmetric disturbances. Here the disturbances lose their ϕ-coordinate dependence. This situation must be considered separately as now the Mach number can be completely scaled out of the stability problem (Duck & Hall 1989). In the lower-deck equations (2.14), to leading order, the pressure gradient term P_X must be retained. The porous-layer admittance now scales as

$$\overline{A_y} = Re^{-1/8}\mu_w^{1/8}T_w^{3/8}\left(M^2-1\right)^{3/8}A_y, \tag{2.21}$$

while the pressure perturbation scales as $(M^2-1)^{-1/4}$ instead of $M^{-3/2}$. This necessitates changes in the factors of M for u and ρ in the upper-deck equations (2.18). The analysis follows that for non-axisymmetric disturbances with M replaced by appropriate powers of (M^2-1).

3. Stability problem

We proceed with analysing the stability of the system of equations described in § 2. We adopt the method of Smith (1979) (see also Smith 1980) who implemented a weakly nonlinear analysis of the stability of an incompressible Blasius boundary layer to Tollmien–Schlichting waves. The objective of the analysis is to monitor the streamwise development of the Tollmien–Schlichting-type (first-mode) disturbances. This problem for the solid-wall case was investigated by Stephen (2006). The planar

case was considered by Seddougui & Bassom (1994). We consider disturbances proportional to

$$E = \exp[\mathrm{i}(\alpha X + n\phi - \Omega\tau)], \tag{3.1}$$

where α is the streamwise wavenumber, Ω is the frequency and n is the azimuthal wavenumber which is an integer $\geqslant 0$. The subsequent analysis is strictly valid for $n > 0$, with the special case of axisymmetric disturbances ($n = 0$) described in § 3.4.

Consider a weakly nonlinear disturbance that is allowed to develop in the vicinity of a linear neutral point (real α, Ω with fixed n). If the relative amplitude of the disturbance in the lower deck is $O(h), h \ll 1$, then Smith (1979, 1980) demonstrated that the scaled amplitude A of the mode will evolve on an $O(h^2)$ length scale. A lower bound on the possible size of h is obtained from Hall & Smith (1984) who demonstrated that to neglect non-parallel effects we must have (for Sutherland's law)

$$O(Re^{-3/32}M^{3/16}T_w^{21/64}) \ll h \ll 1. \tag{3.2}$$

If the lower bound of this inequality is attained, then the length scale over which the disturbance amplitude modulates becomes identical to the length scale over which non-parallelism of the basic flow occurs.

We now take the linear stability of the flow to occur at $x = 1$ and consider a perturbation at the point

$$x = 1 + h^2 x_2. \tag{3.3a}$$

Since the skin friction is a function of x, it will also be slightly perturbed from its neutral value as

$$\lambda = \lambda_1 + h^2\lambda_2, \tag{3.3b}$$

where $\lambda_2 = x_2\,(\mathrm{d}\lambda/\mathrm{d}x)|_{x=1}$. If we were to only consider the linear problem, then λ is a constant and can also be scaled out of the problem as in Cowley & Hall (1990) and Seddougui & Bassom (1997). We fix the azimuthal wavenumber n and allow the frequency to vary as

$$\Omega = \Omega_1 + h^2\Omega_2, \tag{3.3c}$$

where Ω_1 is the neutral value of the frequency obtained from the linear stability problem. To account for the slow streamwise modulation of the amplitude we now introduce a new streamwise coordinate as

$$\tilde{X} = h^2 X. \tag{3.3d}$$

By the method of multiple scales we know that $\partial/\partial X \to (\partial/\partial X) + h^2(\partial/\partial\tilde{X})$. We now seek solutions to our system of equations (2.14) (lower deck) and (2.18) (upper deck). The perturbations imply that for $h \ll 1$ we seek solutions of the form

$$U = (\lambda_1 + h^2\lambda_2)Y + hU_1 + h^2U_2 + h^3U_3 + O(h^4), \tag{3.4a}$$

$$(V, W, P, A, \tilde{p}) = \sum_{j=1}^{3} h^j(V_j, W_j, P_j, A_j, \tilde{p}_j) + O(h^4). \tag{3.4b}$$

Substitution of (3.4) into (2.14) and (2.18) leads to a hierarchy of problems in increasing orders of h which are considered in turn. The details can be found in Michael (2012).

3.1. *First-order: eigenrelation*

The linear stability problem is described by the equations at $O(h)$. The analysis follows that of Seddougui & Bassom (1997). They obtained the eigenrelations that govern the linear stability of the flow for the solid-wall case. This analysis is extended in a straightforward manner for the porous-wall case by incorporating the porous-wall boundary condition. We seek solutions here of the form

$$A_1 = A_{11}E + (\text{c.c.}), \tag{3.5a}$$

where E is given by (3.1) and (c.c.) represents the complex conjugate of the form $A_{11}^c E^{-1}$. The solution to the problem at this order leads to the linear eigenrelation. The details can be found in Seddougui & Bassom (1997) and Stephen & Michael (2012). This equation governs the linear stability of the flow to infinitesimal first-mode disturbances and is given by

$$\frac{\mathrm{Ai}'(\xi_0)}{\displaystyle\int_{\xi_0}^{\infty} \mathrm{Ai}(\xi)\,\mathrm{d}\xi} = (\mathrm{i}\alpha)^{1/3}\left[A_y + \frac{\mathrm{i}n^2}{\alpha a^2}\right]\frac{\mathrm{I}_n(\mathrm{i}\alpha r_s)\mathrm{K}_n(\mathrm{i}\alpha a) - \mathrm{I}_n(\mathrm{i}\alpha a)\mathrm{K}_n(\mathrm{i}\alpha r_s)}{\mathrm{I}_n(\mathrm{i}\alpha r_s)\mathrm{K}_n'(\mathrm{i}\alpha a) - \mathrm{I}_n'(\mathrm{i}\alpha a)\mathrm{K}_n(\mathrm{i}\alpha r_s)}, \tag{3.6}$$

where Ai is the Airy function and I_n and K_n are modified Bessel functions of order n. In obtaining this equation we made the transformation $\xi = (\mathrm{i}\alpha)^{1/3}Y + \xi_0$, where $\xi_0 = -\mathrm{i}\Omega(\mathrm{i}\alpha)^{-2/3}$. The eigenrelation (3.6) is valid for non-axisymmetric disturbance modes. The corresponding relation for axisymmetric disturbances is given in § 3.4. The solid-wall case is recovered by setting $A_y = 0$ in (3.6). For a detailed discussion of the results of the linear stability problem the interested reader is referred to Stephen & Michael (2012).

3.2. *Second-order*

We now proceed to the nonlinear stability of the problem and at $O(h^2)$ seek solutions here in the form

$$A_2 = A_{22}E^2 + A_{22}^c E^{-2} + A_{20}. \tag{3.7}$$

The analysis for solutions to the lower-deck problem follows that of Smith (1979) and is omitted here. The effect of the porous wall comes in through the vertical velocity terms V_{22} and V_{20} evaluated on the cone surface. These terms are zero for the solid-wall problem. The solution to upper-deck problem is obtained in terms of I_{2n} and K_{2n}.

3.3. *Third-order: amplitude equation*

The analysis at $O(h^3)$ will reveal an evolution equation for the unknown amplitude function $A_{11}(\tilde{X})$. The coefficients of the terms in this equation will be complex and they will be evaluated numerically. This in turn will allow us to determine the stabilizing or destabilizing effects of nonlinearity on the flow. We proceed by seeking solutions of the form

$$A_3 = A_{31}E + A_{32}E^2 + A_{33}E^3 + A_{31}^c E^{-1} + A_{32}^c E^{-2} + A_{33}^c E^{-3} + A_{30}. \tag{3.8}$$

The lower-deck equations here are reduced to an inhomogeneous differential equation forced by terms involving the linear solution. We thus need to establish a ‘solvability condition’. The approach is to consider the adjoint of this equation following Hall & Smith (1982). To complete the problem we need to solve the upper-deck problem which is given by an inhomogenous Bessel’s equation. By matching this solution

with that from the lower deck we can obtain the evolution equation for A_{11} in the form

$$a_1 \frac{\mathrm{d}A_{11}}{\mathrm{d}\tilde{X}} = (a_2\lambda_2 + a_3\Omega_2)A_{11} + a_4 A_{11}|A_{11}|^2 . \tag{3.9}$$

The coefficients in (3.9) are complex constants for fixed values of a and r_s and given by

$$\begin{aligned} a_1 = {} & -\mathrm{i}^{4/3}\frac{T1}{\kappa} - \frac{n^2}{\alpha a^2}\frac{\mathrm{Ai}'(\xi_0)}{\kappa}\mathbb{P}_1 \int_{\xi_0}^{\infty} [K(\xi)L(\xi)]\,\mathrm{d}\xi - 2\,(\mathrm{i}\alpha)^{1/3}\,\mathrm{Ai}(\xi_0)\alpha\mathbb{P}_1^{-1} \\ & \times \left[(b_n f_n + c_n d_n)\left\{ \mathrm{K}_n(\mathrm{i}\alpha a) - \frac{\mathrm{Ai}'(\xi_0)}{\kappa}\,(\mathrm{i}\alpha)^{-1/3}\,\mathbb{P}_1 \mathrm{K}_n'(\mathrm{i}\alpha a)\right\}\right. \\ & \left. - (b_n d_n + c_n e_n)\left\{ \mathrm{I}_n(\mathrm{i}\alpha a) - \frac{\mathrm{Ai}'(\xi_0)}{\kappa}\,(\mathrm{i}\alpha)^{-1/3}\,\mathbb{P}_1 \mathrm{I}_n'(\mathrm{i}\alpha a)\right\}\right], \end{aligned} \tag{3.10a}$$

$$a_2 = \mathrm{i}^{-2/3}\alpha L2 + \alpha\kappa^{-1}A_y \mathrm{i}^{1/3} T3, \tag{3.10b}$$

$$a_3 = (\mathrm{i}\alpha)^{1/3}\kappa^{-1}T18, \tag{3.10c}$$

$$a_4 = \frac{\mathrm{i}^{-2/3}\alpha^{5/3}}{\kappa|\kappa|^2}\left[L11 - A_y\left[\alpha^{2/3}\mathbb{P}_1 T22 - \mathbb{P}_2 T25 L12\right] - A_y^c \mathbb{P}_1^c L13\right], \tag{3.10d}$$

where $\kappa = \int_{\xi_0}^{\infty} \mathrm{Ai}(s)\,\mathrm{d}s$, $\mathbb{P}_1 = (A_y + (\mathrm{i}n^2/\alpha a^2))^{-1}$, $\mathbb{P}_2 = (A_y + 2(\mathrm{i}n^2/\alpha a^2))^{-1}$; $K(\xi)$ and $L(\xi)$ are terms from the adjoint equation and defined in Bassom (1989); b_n to f_n are constants (defined in Stephen 2006) that depend on the neutral values of α for fixed values of a and r_s and involve modified Bessel functions. All other abbreviations *Tij*, *Lij* are defined in the Appendix.

3.4. *Axisymmetric problem*

We again consider the case of axisymmetric disturbances separately. For these disturbances the corresponding linear eigenrelation can be obtained as

$$\frac{\mathrm{Ai}'(\xi_0)}{\displaystyle\int_{\xi_0}^{\infty}\mathrm{Ai}(\xi)\,\mathrm{d}\xi} = -(\mathrm{i}\alpha)^{1/3}\left[A_y + \mathrm{i}\alpha\right]\frac{\mathrm{I}_0(\mathrm{i}\alpha r_s)\mathrm{K}_0(\mathrm{i}\alpha a) - \mathrm{I}_0(\mathrm{i}\alpha a)\mathrm{K}_0(\mathrm{i}\alpha r_s)}{\mathrm{I}_0(\mathrm{i}\alpha r_s)\mathrm{K}_1(\mathrm{i}\alpha a) + \mathrm{I}_1(\mathrm{i}\alpha a)\mathrm{K}_0(\mathrm{i}\alpha r_s)}. \tag{3.11}$$

At the third-order we consider solutions for fixed frequency Ω, thus the resulting amplitude equation is

$$a_{10}\frac{\mathrm{d}A_{11}}{\mathrm{d}\tilde{X}} = a_{20}\lambda_2 A_{11} + a_{40}A_{11}|A_{11}|^2 . \tag{3.12}$$

The analysis at third order is carried out in a similar fashion to the non-axisymmetric case. The solution obtained is similar to the non-axisymmetric solution, but with all the terms now functions of modified Bessel functions of order zero. The coefficients in (3.12) may be expressed as

$$\begin{aligned} a_{10} = {} & -\mathrm{i}^{4/3}\frac{T1}{\kappa} - 2\,(\mathrm{i}\alpha)^{1/3}\,\mathrm{Ai}(\xi_0)\alpha\mathbb{P}_{10}^{-1} \\ & \times \left[(b_0 f_0 + c_0 d_0)\left\{ \mathrm{K}_0(\mathrm{i}\alpha a) - \frac{\mathrm{Ai}'(\xi_0)}{\kappa}\,(\mathrm{i}\alpha)^{-1/3}\,\mathbb{P}_{10}\mathrm{K}_0'(\mathrm{i}\alpha a)\right\}\right. \\ & \left. - (b_0 d_0 + c_0 e_0)\left\{ \mathrm{I}_0(\mathrm{i}\alpha a) - \frac{\mathrm{Ai}'(\xi_0)}{\kappa}\,(\mathrm{i}\alpha)^{-1/3}\,\mathbb{P}_{10}\mathrm{I}_0'(\mathrm{i}\alpha a)\right\}\right], \end{aligned} \tag{3.13a}$$

$$a_{20} = \mathrm{i}^{-2/3}\alpha L2 + \alpha\kappa^{-1}A_y\mathrm{i}^{1/3}T3, \tag{3.13b}$$

$$a_{40} = \frac{\mathrm{i}^{-2/3}\alpha^{5/3}}{\kappa|\kappa|^2}\left[L11^0 - A_y\left[\alpha^{2/3}\mathbb{P}_{10}T22 - \mathbb{P}_{20}T25L12^0\right] - A_y^c\mathbb{P}_{10}^c L13^0\right], \tag{3.13c}$$

where the corresponding axisymmetric versions of the abbreviations $\mathbb{P}_i$, Lij are defined in the Appendix.

4. Nonlinear stability results

We will begin this section by presenting the results of the nonlinear stability analysis for the solid wall with flow parameters corresponding to the experiments of Maslov (2003) and Fedorov *et al.* (2006). This was not done by Stephen (2006). We will then present corresponding results obtained using the different porous-wall models and deduce the effect of the porous walls on the nonlinear stability. A relationship between the angular frequency of disturbances propagating through the pore (ω) and the first-mode disturbance frequency (Ω) (in the lower deck) is obtained. This accounts for the fact that Ω^* is non-dimensionalized using the streamwise distance L^* as the reference length and that ω^* is non-dimensionalized using the boundary-layer displacement thickness δ^*. For non-axisymmetric disturbances we have

$$\omega = \frac{R}{Re}\left[Re^{1/4}\mu_w^{-1/4}T_w^{-3/4}M^{-1/2}\right]\Omega, \tag{4.1}$$

and for axisymmetric disturbances

$$\omega = \frac{R}{Re}\left[Re^{1/4}\mu_w^{-1/4}T_w^{-3/4}\left(M^2-1\right)^{1/4}\right]\Omega, \tag{4.2}$$

where R is the Reynolds number based on the boundary-layer displacement thickness. These scalings are used to find ω corresponding to Ω used in the calculations.

4.1. *Solid wall*

In order to present our results in regimes of practical interest, we will use the flow parameters from the relevant experimental studies. We take $M = 5.3$, $Re_1 = 15.2 \times 10^6$, $T_-^* = 56.4$ K, $Pr = 0.708$, $\gamma = 1.4$ and the cone wall temperature to be at the adiabatic temperature. The cone angle and Mach number from the experiments will determine the shock angle θ_s and the scaled cone radius a. Using $\theta_c = 7^\circ$ and $M_\infty = 6$ in (2.1) gives $\sigma = 12.3^\circ$ which matches the lower bound of (2.11). Once the shock angle has been determined, the ratio a/r_s may be obtained from geometric arguments. We find for a slender cone of half-angle $\theta_c = 7^\circ$ and $M_\infty = 6$ that

$$\frac{a}{r_s} \approx \frac{\sin\theta_c}{\tan\theta_s + \sin\theta_c} = 0.57, \tag{4.3}$$

where we have taken $\cos\theta_c \approx 1$ and $\theta_s = 5.3^\circ$. Thus all our results are presented for $a/r_s = 0.57$. We consider $0 < a < 5$, which corresponds to $0 < L^* < 14$ m for non-axisymmetric modes.

We turn to the non-axisymmetric problem and the evolution equation (3.9). We can solve this equation using separation of variables. Following Stuart (1960) we can determine an explicit expression for the amplitude $|A_{11}|^2$ as

$$|A_{11}|^2 = \frac{2\mathscr{K}\mathrm{e}^{\mathscr{K}\tilde{X}}}{\left[\mathscr{K}C_1 - 2\mathrm{Re}\left(\dfrac{a_4}{a_1}\right)\mathrm{e}^{\mathscr{K}\tilde{X}}\right]}, \tag{4.4a}$$

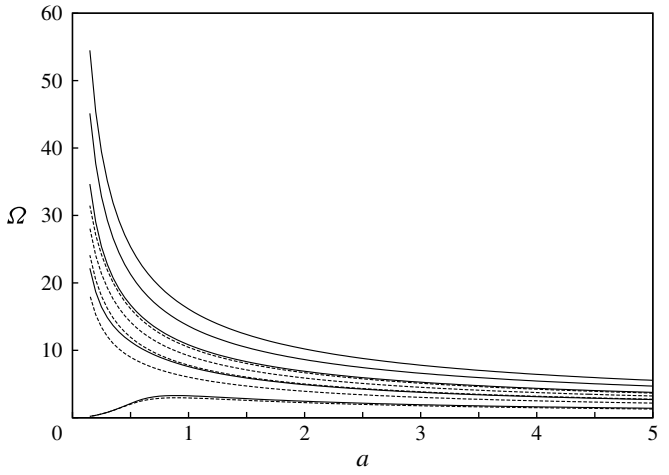

FIGURE 2. The first five neutral modes of (3.6) with $n = 1$. Shown is Ω against local cone radius a for $a/r_s = 0.57$:—, solid wall; - - -, regular microstructure model (2.5).

where $\mathscr{K} = 2\mathrm{Re}\,((a_2/a_1)\lambda_2 + (a_3/a_1)\Omega_2)$ and C_1 is a constant of integration. When $\mathscr{K} > 0$ we have linear instability. Note that λ_2 is negative downstream of the neutral location. If $\mathrm{Re}\,(a_4/a_1) > 0$, the nonlinear effects are destabilizing and we have subcritical instability where there is a threshold amplitude between disturbances growing or decaying. If $\mathrm{Re}\,(a_4/a_1) < 0$, nonlinear effects are stabilizing and the linearly unstable mode is supercritically stable with an equilibrium amplitude given by

$$|A_{11}| = \sqrt{\frac{\mathrm{Re}\left(\dfrac{a_2}{a_1}\lambda_2 + \dfrac{a_3}{a_1}\Omega_2\right)}{-\mathrm{Re}\left(\dfrac{a_4}{a_1}\right)}}. \tag{4.4b}$$

Typical neutral solutions for solid and regular porous microstructure cases are shown in figure 2 for Ω with $n = 1$. Details of the porous parameters used are given in § 4.2 below. The presence of the shock allows multiple neutral modes. Here regions of instability lie above the curve. We can see in figure 2 that the neutral values of Ω are lower for the porous wall than for the solid wall. Thus, there is a destabilizing effect in that disturbances of lower frequencies can become unstable. This effect is greater for the higher modes. The results for spatial growth rates shown in Stephen & Michael (2012) show that the porous wall leads to larger unstable growth rates.

In figure 3(*a*) we show $\mathrm{Re}(a_2/a_1)$ as a function of a for $n = 1$ corresponding to the first five neutral modes of (3.6) for a solid wall. The arrows here and on all the subsequent figures indicate increasing mode number. We can see that this quantity is always negative. The results for $n = 2$ are shown in figure 4(*a*). The magnitudes are decreased when compared to $n = 1$. The corresponding values of $\mathrm{Re}(a_3/a_1)$ are shown in figures 3(*b*) and 4(*b*), respectively for $n = 1$ and $n = 2$. There is a difference in behaviour of $\mathrm{Re}(a_3/a_1)$ for the first mode for small values of a, corresponding to the anomalous behaviour of the lowest neutral solution; see figure 2. The effect of increasing the azimuthal wavenumber is to decrease the magnitude of $\mathrm{Re}(a_3/a_1)$.

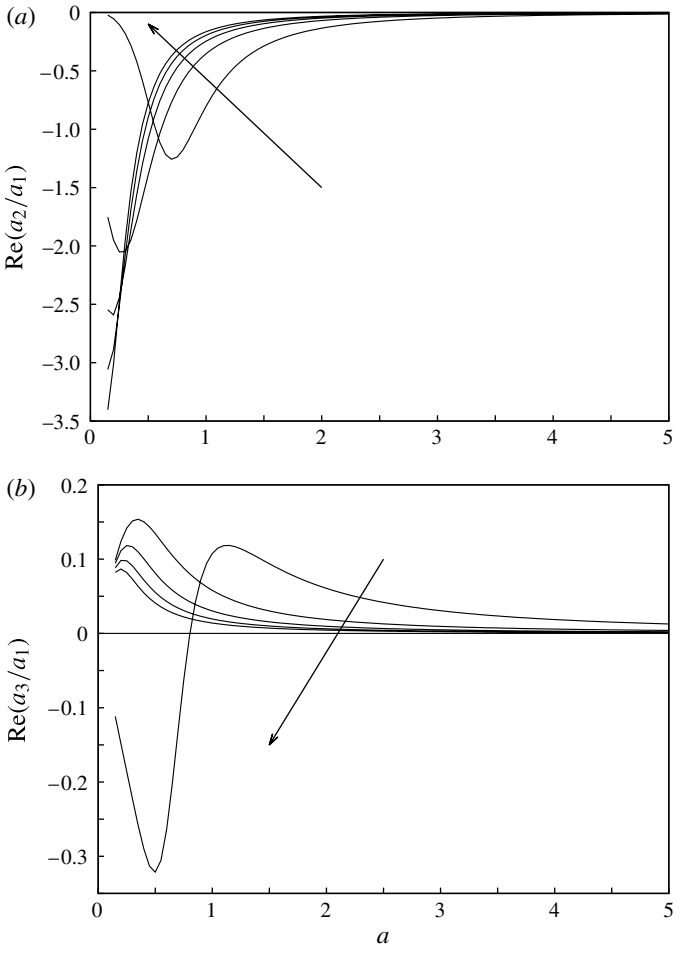

FIGURE 3. (*a*) $\mathrm{Re}(a_2/a_1)$ and (*b*) $\mathrm{Re}(a_3/a_1)$, as a function of local cone radius a for the first five modes. Results are shown for a solid wall with $n = 1$ and $a/r_s = 0.57$.

We now investigate the effect of nonlinearity on linearly unstable disturbances by considering the sign of $\mathrm{Re}(a_4/a_1)$. In order to see the behaviour of the different modes the value of $\mathrm{Re}(a_4/a_1)$ versus a for $0 \leqslant a \leqslant 1$ is shown in figure 5(*a*) and versus a for $1 \leqslant a \leqslant 5$ is shown in figure 5(*b*) for $n = 1$. In figure 5(*a*,*b*) we can see that the sign of $\mathrm{Re}(a_4/a_1)$ is always positive for the first mode ($m = 1$). Thus nonlinear effects always destabilize this mode, possibly leading to a subcritical instability. The effect of nonlinearity on the remaining four modes depends on the value of a. For $a < 1$, $\mathrm{Re}(a_4/a_1) < 0$ leading to supercritical instability. As the value of a increases, the sign of $\mathrm{Re}(a_4/a_1)$ becomes positive beginning with the higher modes indicating that nonlinear effects now destabilize these linearly unstable modes. In the limit of large a we can see that $\mathrm{Re}(a_4/a_1) \to 0$ for all the modes, with the first mode having the highest amplitude. Recall that for a fixed cone angle the effect of increasing a is to move further along the cone surface. Thus at large streamwise distances we can expect nonlinear disturbance amplitudes to be very small. The corresponding results for $\mathrm{Re}(a_4/a_1)$ with $n = 2$ can be seen in figures 6 and 7. In figure 6 we can see

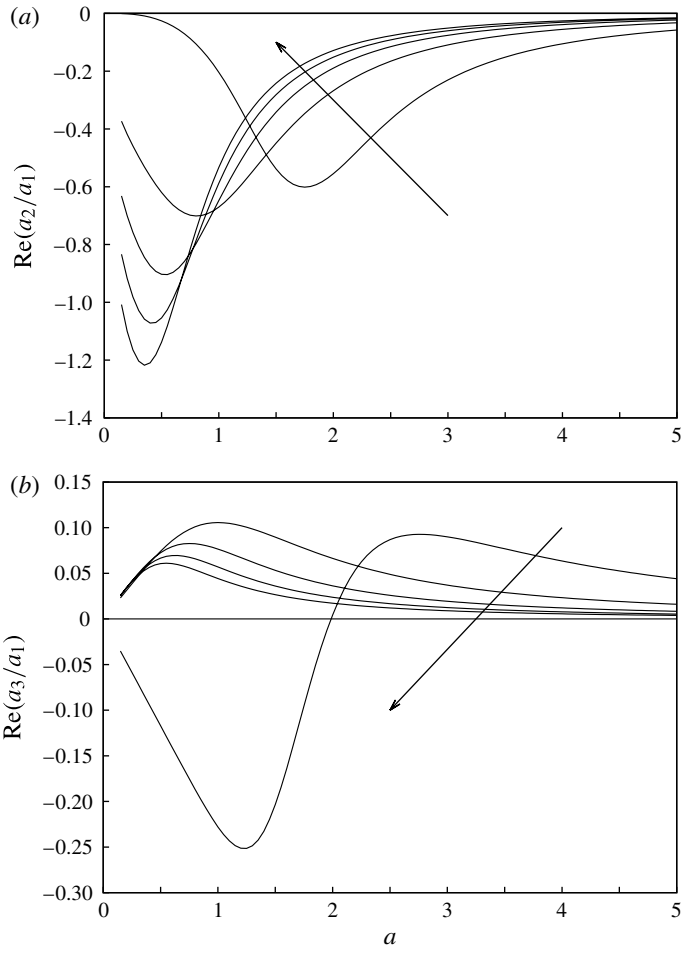

FIGURE 4. (*a*) $\mathrm{Re}(a_2/a_1)$ and (*b*) $\mathrm{Re}(a_3/a_1)$, as a function of local cone radius a for the first five modes. Results are shown for a solid wall with $n = 2$ and $a/r_s = 0.57$.

that the effects of nonlinearity on mode numbers > 1 for $n = 2$ are similar to that for $n = 1$. Higher azimuthal wavenumber allows the stabilizing effect of nonlinearity to persist for larger ranges of a. In figure 7 we see that $\mathrm{Re}(a_4/a_1)$ becomes positive for $a > 2.3$ with the higher modes becoming destabilized first. The effect of azimuthal wavenumber is more significant on the first mode as can be seen in the inset of figure 6. Here we see that the first mode is stabilized by nonlinearity for a narrow range of a ($\mathrm{Re}(a_4/a_1) < 0$ when $1.6 < a < 3.3$). In the limit of large a nonlinear effects on the first mode persist while the effects on the higher modes diminish as $\mathrm{Re}(a_4/a_1)$ remains small for these modes. The effect of nonlinearity for disturbances with $n = 3$ have also been investigated. The results (not shown) indicate that overall trends remain similar to that for $n = 2$. We may thus conclude that nonlinear effects tend to stabilize the higher modes for a wider range of a for higher azimuthal wavenumbers, and the first mode becomes the most destabilized by nonlinearity at large values of a.

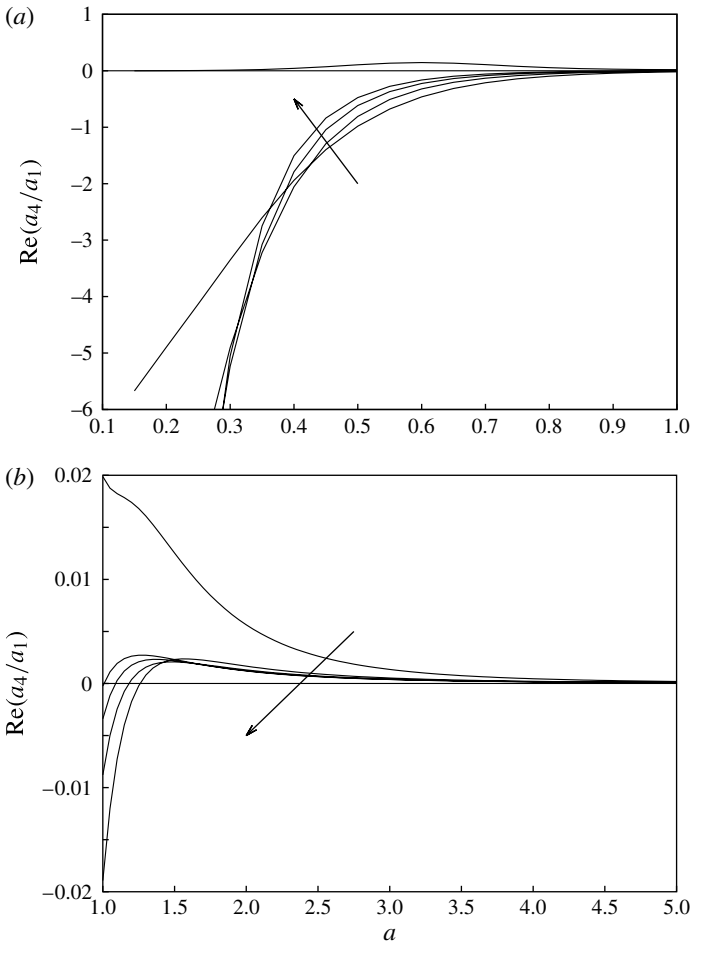

FIGURE 5. $\mathrm{Re}(a_4/a_1)$ for the first five modes as a function of local cone radius a for (a) $0 \leqslant a \leqslant 1.0$; ($b$) $1.0 \leqslant a \leqslant 5.0$. Results are shown for a solid wall with $n = 1$ and $a/r_s = 0.57$.

We consider the effect of nonlinearity on axisymmetric disturbances next. The axisymmetric equivalent of figure 2 is shown in figure 8 where the neutral values of Ω are shown as a function of a for $a/r_s = 0.57$ for the first four modes. The overall features remain the same as the non-axisymmetric case. The destabilizing effect of the porous wall is smaller when compared to its effect on non-axisymmetric disturbances. Axisymmetric disturbances are linearly unstable if $\mathrm{Re}(a_{20}\lambda_2/a_{10}) > 0$. If $\mathrm{Re}(a_{40}/a_{10}) < 0$ for these disturbances then nonlinear effects are stabilizing and the linearly unstable modes are supercritically stable with an equilibrium amplitude

$$|A_{11}| = (-\lambda_2)^{1/2}\left(\frac{-\mathrm{Re}(a_{20})}{-\mathrm{Re}(a_{40})}\right)^{1/2}. \tag{4.5}$$

In figure 9(a) we can see $\mathrm{Re}(a_{20}/a_{10})$ as a function of a for the first four modes. We notice that this quantity is always negative so disturbances are linearly unstable. Figure 9(b) shows $\mathrm{Re}(a_{40}/a_{10})$ versus a. We see that this quantity is negative for all the modes with the exception of the first mode. For this mode $\mathrm{Re}(a_{40}/a_{10})$ becomes

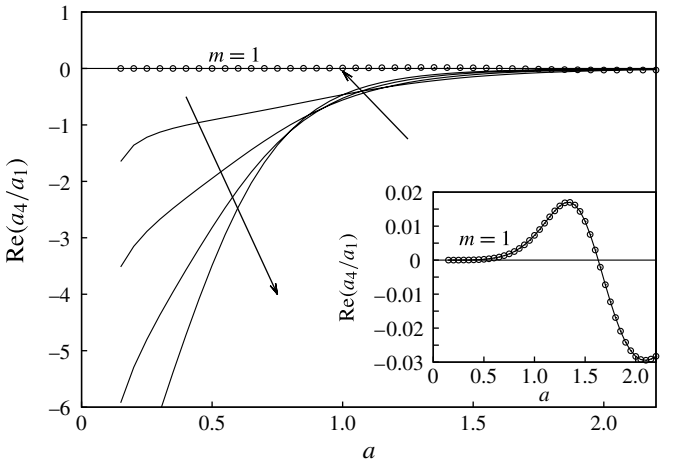

FIGURE 6. $\mathrm{Re}(a_4/a_1)$ for the first five modes as a function of local cone radius a for $0 \leqslant a \leqslant 2.3$. Results are shown for a solid wall with $n = 2$ and $a/r_s = 0.57$. Inset: $\mathrm{Re}(a_4/a_1)$ for the first mode as a function of a.

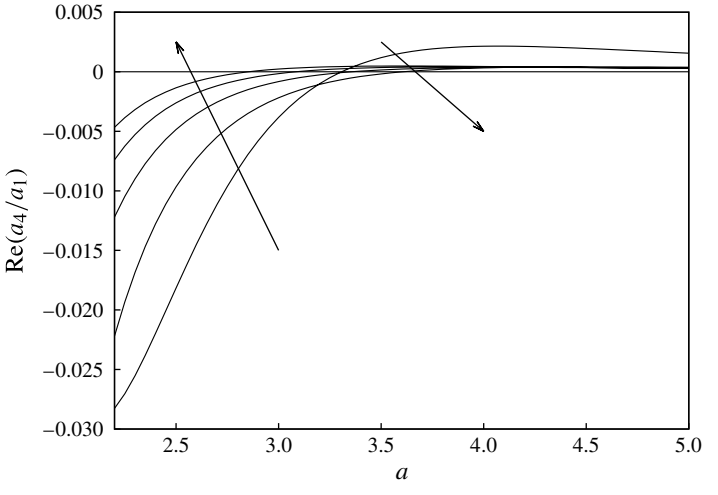

FIGURE 7. $\mathrm{Re}(a_4/a_1)$ for the first five modes as a function of local cone radius a for $2.3 \leqslant a \leqslant 5.0$. Results are shown for a solid wall with $n = 2$ and $a/r_s = 0.57$.

slightly positive for $a > 2.3$. Thus, we can expect nonlinear effects to stabilize linearly unstable axisymmetric disturbances with the exception of the first mode which is slightly destabilized above a certain value of a.

The results discussed above for $\mathrm{Re}(a_{40}/a_{10})$ and $\mathrm{Re}(a_4/a_1)$ differ from those presented by Stephen (2006). In that paper it was reported that $\mathrm{Re}(a_{40}/a_{10})$ and $\mathrm{Re}(a_4/a_1)$ were always negative, so the nonlinear effects were always stabilizing. Our results correcting the numerical error in Stephen (2006) have shown the significant result that the nonlinear effects are destabilizing for particular ranges of a.

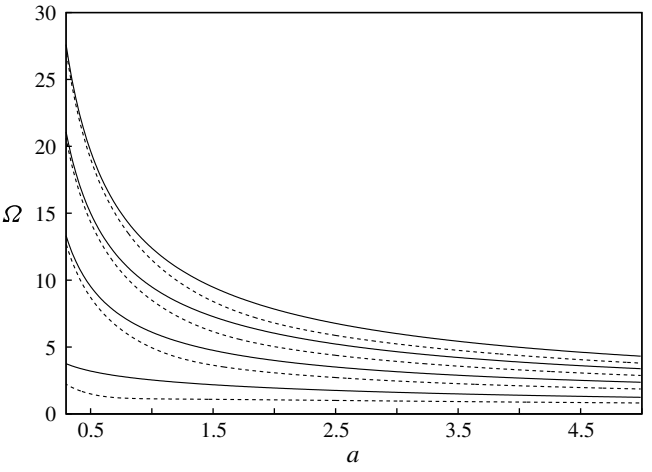

FIGURE 8. The first four neutral modes of (3.11). Shown is Ω against local cone radius a for $a/r_s = 0.57$ and $n = 0$: —, solid wall; - - -, regular microstructure model (2.5).

4.1.1. *Effect of the shock*

Before proceeding to investigate the effect of porous walls on the nonlinear stability it is useful to consider the stability problem in the absence of a shock. The problem in the absence of a shock was first considered by Duck & Hall (1989, 1990). It can be shown that the neutral curves in the absence of a shock differ fundamentally from those in the presence of shock as solutions are only possible for a finite range of a (Seddougui & Bassom 1997). This is because if no shock is present, solutions to (2.18) at first-order are only proportional to $\mathrm{K}_n(\mathrm{i}\alpha r)$, allowing only outgoing waves as $r \to \infty$. This modifies the resulting eigenrelation. The nonlinear stability analysis can be carried out in a straightforward manner for this problem. Figure 10 shows $\mathrm{Re}(a_4/a_1)$ as a function of a for $n = 1$ and $n = 2$. It can be seen that the sign of $\mathrm{Re}(a_4/a_1)$ is always negative and two solution branches exist for $0 < a < 0.75$ for $n = 1$ and $0 < a < 1.75$ for $n = 2$. Thus in the absence of a shock nonlinear effects are stabilizing for all admissible values of a.

4.2. *Effect of porous walls*

We now investigate the effect of porous coatings. First of all, the results using the regular microstructure model comprising a regular array of cylindrical pores of circular cross-section are compared to the results for a solid wall for non-axisymmetric modes. The flow conditions match the experimental conditions of Maslov (2003). The porous parameters are pore radius $r_p^* = 28.5$ μm, porosity $\phi_0 = 0.2$ and pore depth $h^* = 450$ μm. Neutral results for $n = 1$ were presented in figure 2 which showed that the porous wall reduces the neutral values of Ω. The porous wall has only a small effect on the neutral values of α (not shown). The corresponding results for $n = 2$ are shown in figure 11. We can again notice the destabilizing effect of the porous wall. The difference between the neutral curves of the solid and porous walls is smaller for $n = 2$ compared to $n = 1$ especially for the lower neutral curves. To investigate the effect of nonlinearity we turn to figure 12 which compares $\mathrm{Re}(a_4/a_1)$ for $n = 1$ between the solid and regular porous walls for the first five modes ($m = 1$–5). We see that nonlinear effects are enhanced by the porous wall giving larger values of

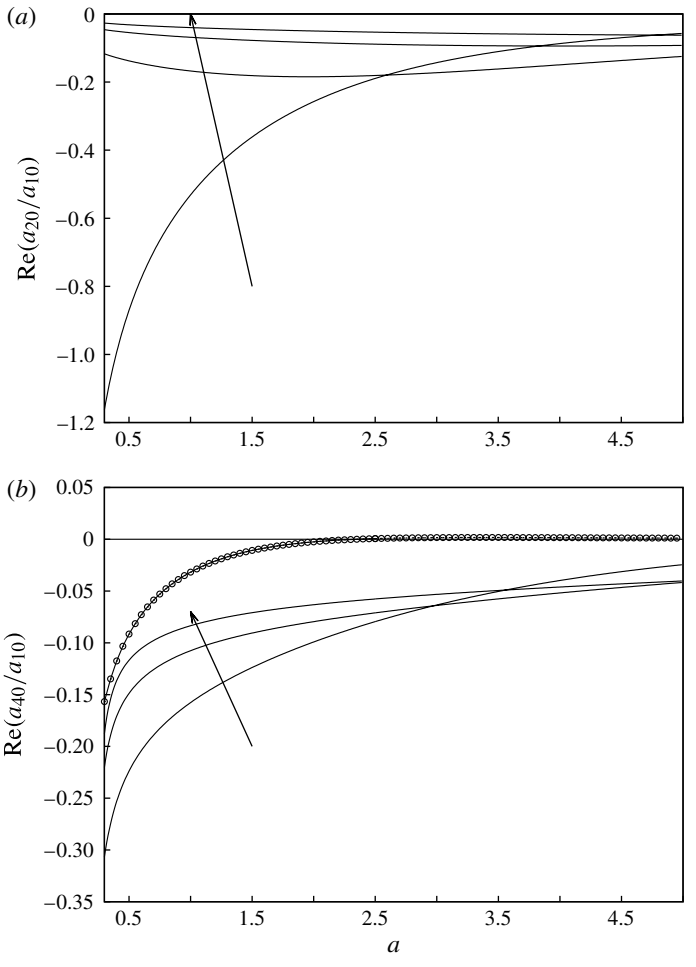

FIGURE 9. (*a*) $\mathrm{Re}(a_{20}/a_{10})$ and (*b*) $\mathrm{Re}(a_{40}/a_{10})$ for the first four modes as a function of local cone radius a. Results are shown for a solid wall with $n = 0$ and $a/r_s = 0.57$. Results for the first mode are indicated by ∘.

$\mathrm{Re}(a_4/a_1)$. In the presence of the porous wall nonlinear effects destabilize the lower modes (first and second) while stabilizing the higher modes (three to five). We can see this from the fact that $\mathrm{Re}(a_4/a_1)$ for the porous wall has larger positive values for the first and second modes compared to the solid wall and that $\mathrm{Re}(a_4/a_1)$ for the porous wall becomes positive at larger values of a compared with the solid wall for the higher modes. However once destabilized, the higher modes of the porous wall have larger values of $\mathrm{Re}(a_4/a_1)$ compared to the solid wall. For large enough values of a, we can expect the nonlinear effects to diminish just as in the solid wall case. Figure 13 shows the corresponding results for $\mathrm{Re}(a_4/a_1)$ with $n = 2$. Here we see that nonlinearity destabilizes the first, second, third and fourth modes in comparison to corresponding modes of the solid wall, while stabilizing the fifth and possibly higher modes of the porous wall. Results obtained for $n = 3$ (not shown) show that nonlinearity destabilizes all of the first five modes of the porous wall compared to the solid wall. We can thus infer that in the presence of the porous wall, nonlinearity destabilizes lower modes,

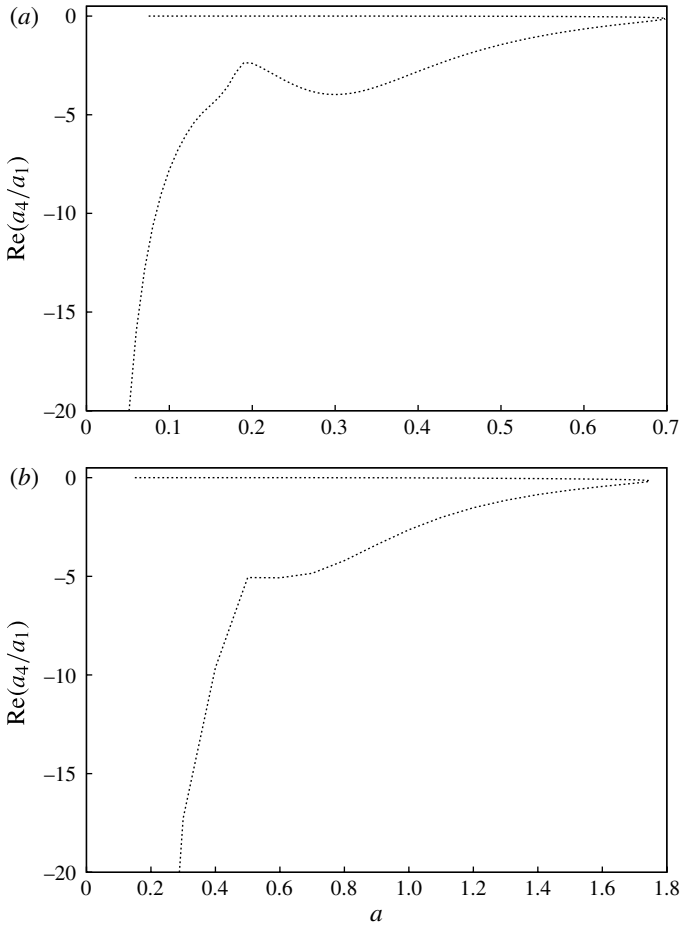

FIGURE 10. $\mathrm{Re}(a_4/a_1)$ as a function of local cone radius a in the absence of shock. Results are shown for solid wall with (a) $n = 1$ and (b) $n = 2$.

with their mode number increasing with azimuthal wavenumber. Thus disturbances of large enough amplitude could lead to transition to turbulence.

We now compare the effect of porosity on the nonlinear stability of axisymmetric disturbances. Looking at figure 14 which shows $\mathrm{Re}(a_{40}/a_{10})$ as a function of a for the porous wall and solid wall, we see that in the presence of the porous wall all the modes are destabilized by nonlinearity with the most significant effect being felt by the first mode. This mode is destabilized for all values of a.

Next we consider the random microstructure model of (2.9). The results using this model are compared with those obtained using the regular microstructure model. The porosity of the felt metal is taken to be 0.75 and the fibre diameter is 30 μm. For comparison the regular microstructure model is used with a porosity of 0.2 and pore radius of 30 μm. In figure 15 we see that, with the exception of the first mode, neutral values of Ω for the felt metal are significantly lower than the corresponding ones for the regular porous model. This is mainly as a result of the larger value of porosity for the felt metal (see Stephen & Michael 2012 for more discussion). Figure 16 shows $\mathrm{Re}(a_4/a_1)$ for $n = 1$ for both models. We see that nonlinear effects destabilize the first

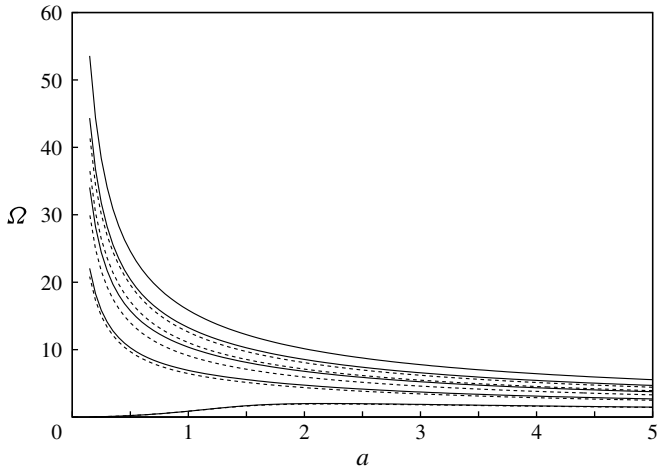

FIGURE 11. The first five neutral modes of (3.6) with $n = 2$. Shown is frequency Ω against local cone radius a for $a/r_s = 0.57$: —, solid wall; - - -, regular microstructure model (2.5).

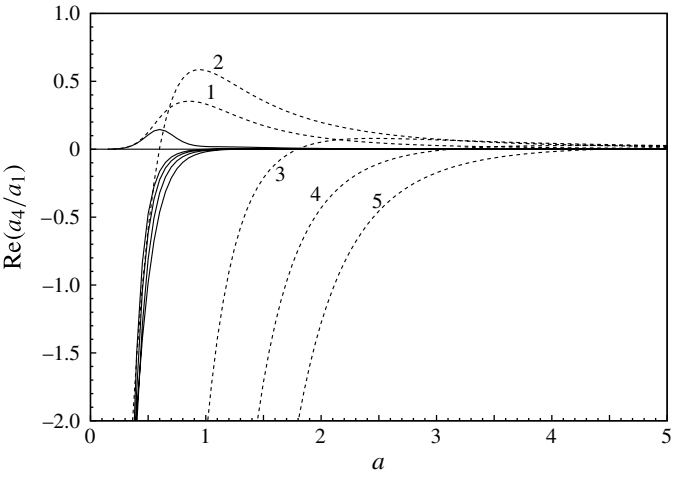

FIGURE 12. $\mathrm{Re}(a_4/a_1)$ for the first five modes as a function of local cone radius a for $n = 1$ and $a/r_s = 0.57$: —, solid wall; - - -, regular microstructure model (2.5).

two modes of the felt metal model when compared to the regular porous model. The effect on the higher modes is opposite as we see that $\mathrm{Re}(a_4/a_1)$ becomes positive for smaller values of a for the regular porous model as compared to the felt metal model. Once destabilized, values of $\mathrm{Re}(a_4/a_1)$ are more positive for the felt metal indicating that nonlinear amplification of disturbances will be stronger. Similar trends are also observed (not shown) for the case of axisymmetric disturbances.

Finally we consider the mesh microstructure model of (2.7). The results using this model are compared with those obtained using the regular microstructure model. The porosity of the mesh model is 0.8, and width of each pore section is 100 μm. For comparison the regular porous model is used with a porosity of 0.2 and pore radius of

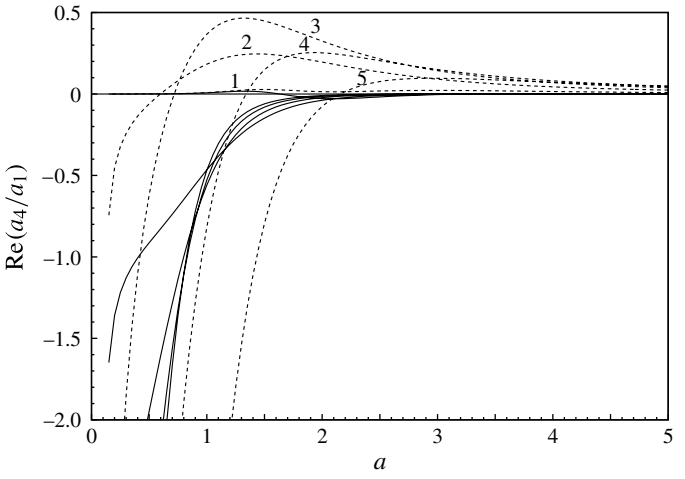

FIGURE 13. $\mathrm{Re}(a_4/a_1)$ for the first five modes as a function of local cone radius a for $n = 2$ and $a/r_s = 0.57$: —, solid wall; - - -, regular microstructure model (2.5).

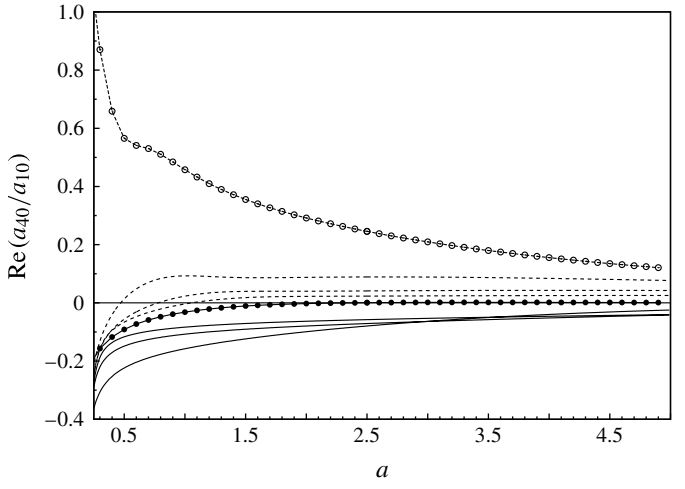

FIGURE 14. $\mathrm{Re}(a_{40}/a_{10})$ for the first four modes as a function of local cone radius a for $n = 0$ and $a/r_s = 0.57$: —, solid wall; - - -, regular microstructure model (2.5). Results for the first mode are indicated by • for solid wall and ○ for porous wall.

30 μm. In figure 17 we can see that neutral curves corresponding to the mesh model are slightly lower than the corresponding ones for the regular porous model. Figure 18 shows $\mathrm{Re}(a_4/a_1)$ for $n = 1$ for both models. The effect of the two models on the first mode is similar with the stabilizing effects of nonlinearity being stronger for the mesh model compared to the regular model. For the higher modes nonlinear effects are slightly more destabilizing for the regular model compared to the mesh model. This can again be seen by noting that $\mathrm{Re}(a_4/a_1)$ becomes positive for smaller values of a for the regular model compared to the mesh model. At large values of a, $\mathrm{Re}(a_4/a_1)$ is more positive for the mesh model for the first four modes while for the fifth and

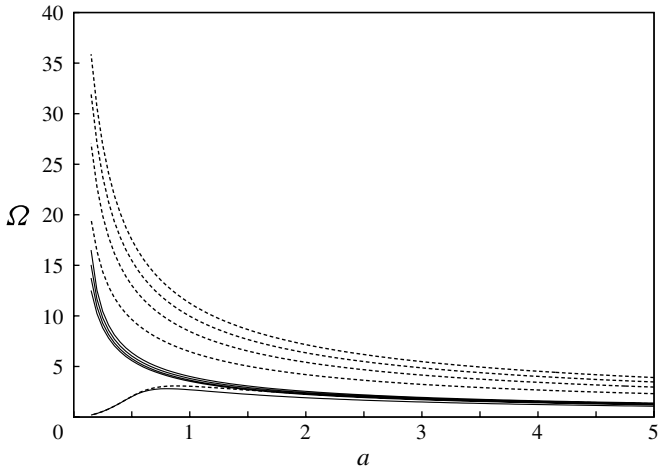

FIGURE 15. The first five neutral modes of (3.6) with $n = 1$. Shown is frequency Ω against local cone radius a for $a/r_s = 0.57$: —, random microstructure model (2.9); - - -, regular microstructure model (2.5).

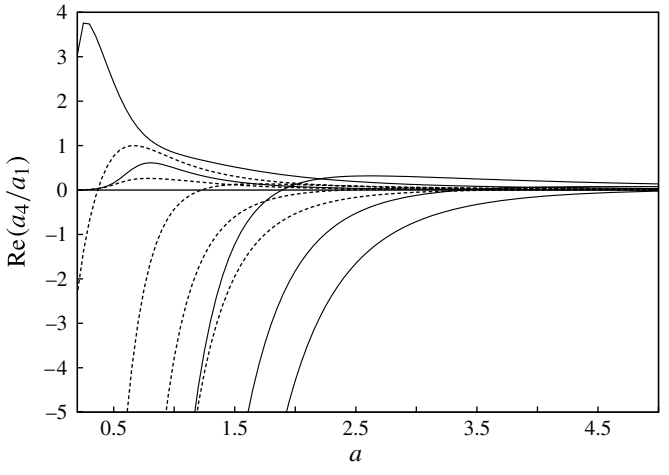

FIGURE 16. $\mathrm{Re}(a_4/a_1)$ for the first five modes as a function of local cone radius a for $n = 1$ and $a/r_s = 0.57$: —, random microstructure model (2.9); - - -, regular microstructure model (2.5).

possibly higher modes $\mathrm{Re}(a_4/a_1)$ is larger for the regular model. Corresponding results for axisymmetric disturbances (not shown) indicate very slight differences between the effects of the two models.

5. Discussion

The weakly nonlinear stability of the first Mack mode (viscous) disturbances in the hypersonic boundary layer on a sharp slender cone with passive porous walls has been investigated. The analysis shows that small-amplitude linearly unstable disturbances can either evolve from the linear neutral point towards an equilibrium amplitude or

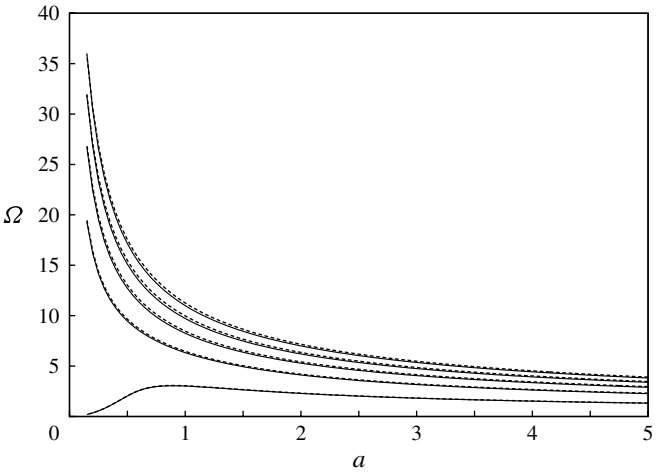

FIGURE 17. The first five neutral modes of (3.6) with $n = 1$. Shown is frequency Ω against local cone radius a for $a/r_s = 0.57$: —, mesh microstructure model (2.7); - - -, regular microstructure model (2.5).

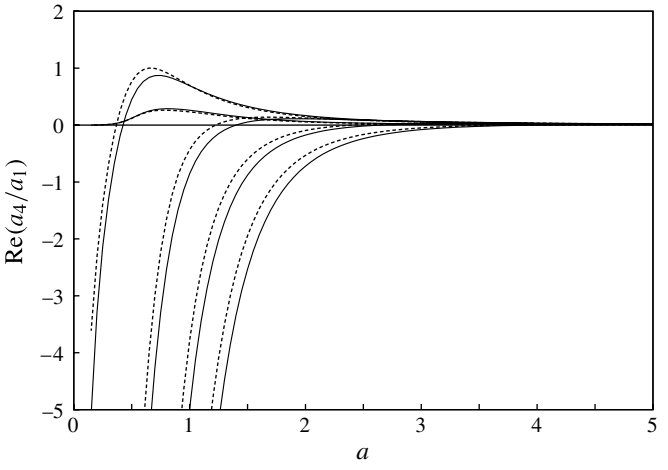

FIGURE 18. $\mathrm{Re}(a_4/a_1)$ for the first five modes as a function of local cone radius a for $n = 1$ and $a/r_s = 0.57$: —, mesh microstructure model (2.7); - - -, regular microstructure model (2.5).

there is a threshold amplitude. The stability of this disturbance is dependent on the mode number and the local cone radius a where the viscous–inviscid interaction takes place. There are two situations depending on whether $\mathrm{Re}(a_4/a_1)$ is negative or positive for a particular value of a. If $\mathrm{Re}(a_4/a_1) < 0$ we have supercritical instability and an equilibrium amplitude so linearly unstable disturbances grow but saturate. If $\mathrm{Re}(a_4/a_1) > 0$ then we have subcritical instability and an initial threshold amplitude. Disturbances with amplitude smaller than this threshold grow but ultimately decay. For disturbances larger than this threshold there will be unbounded growth. Thus, in the latter case nonlinear effects could lead a finite-amplitude mode towards breakdown and

transition to turbulence. Thus, the size of the incoming disturbances is important in leading to transition to turbulence. The analysis here reveals the particular values of a for which the equilibrium state is subcritically unstable. Here nonlinearity enhances the amplification of a small-amplitude disturbance proportional to E that interacts with its harmonic, E^2 and mean flow disturbance, E^0. The effect of the attached shock is found to be significant. The presence of the shock leads to multiple unstable modes for all values of a. In the absence of a shock, unstable solutions are possible only for a finite range of cone radius a and nonlinearity stabilizes linearly unstable disturbances for all admissible values of a.

For axisymmetric disturbances on a solid wall, nonlinear effects tend to stabilize all higher modes, while the lowest mode is slightly destabilized when a becomes large enough. In the presence of the porous wall all the modes are destabilized when compared to those on the solid wall. Linear stability results (Stephen & Michael 2012) show that the lowest mode is the most unstable and has the largest spatial growth rates for both solid and porous walls. This most dangerous mode is also the most destabilized by nonlinearity in the presence of the porous wall. For non-axisymmetric disturbances on a solid wall, nonlinear effects destabilize the lowest mode, while the higher modes are stabilized up to a certain value of a which increases with azimuthal wavenumber. All porous-wall models considered destabilize the neutral modes. When considering the effect of nonlinearity on linearly unstable modes, we can state that lower modes are greatly destabilized by nonlinearity while it has a stabilizing effect on the higher modes. Stephen & Michael (2012) show that it is the higher modes that have the largest spatial growth rates in the presence of the porous wall. The effect of nonlinearity is to stabilize these most linearly amplified modes by pushing the point of subcritical instability to larger values of a.

The random microstructure felt metal model was compared with the regular porous model. The felt metal significantly destabilizes the neutral modes and strongly amplifies the linearly unstable modes with the higher modes giving the largest growth rates (Stephen & Michael 2012). Nonlinear effects in the presence of the felt metal wall stabilize these more dangerous higher modes over a larger range of a while destabilizing the more slowly growing lower modes. When comparing the difference between the mesh microstructure model and the regular porous model, we notice similar effects for both models on all the modes. The regular porous model slightly destabilizes all modes when compared to the mesh model. Since the felt metal and mesh coating have higher porosity, to corroborate these findings, nonlinear stability results for the regular porous model with a higher porosity of $\phi_0 = \pi/4$ were obtained. In figures 19(a) and 19(b) for $n = 0$ and $n = 1$ respectively, we see that higher porosity leads to nonlinearity having a stabilizing effect on mode numbers greater than one. This is a result of the increase in the value of a at which $\mathrm{Re}(a_4/a_1)$ becomes positive. However, for large values of a the destabilizing effect of nonlinearity is stronger, with $\mathrm{Re}(a_4/a_1)$ being slightly larger for higher porosity. In figure 20(a) for $n = 2$ we see the stabilizing effect for mode numbers greater than two and in figure 20(b) for $n = 3$ we see it for mode numbers greater than three. Thus porous coatings with higher porosity allow nonlinear effects to stabilize higher mode number disturbances at a particular location, with the mode number of the lowest mode that is stabilized increasing with increasing azimuthal wavenumber.

We can deduce the significance of curvature on the nonlinear stability by comparing our results for a solid wall to those obtained from the analysis of Seddougui & Bassom (1994) for the weakly nonlinear stability of flow over a wedge. Figure 21 shows the variation of $\mathrm{Re}(a_3)$, the coefficient of the nonlinear term of the amplitude

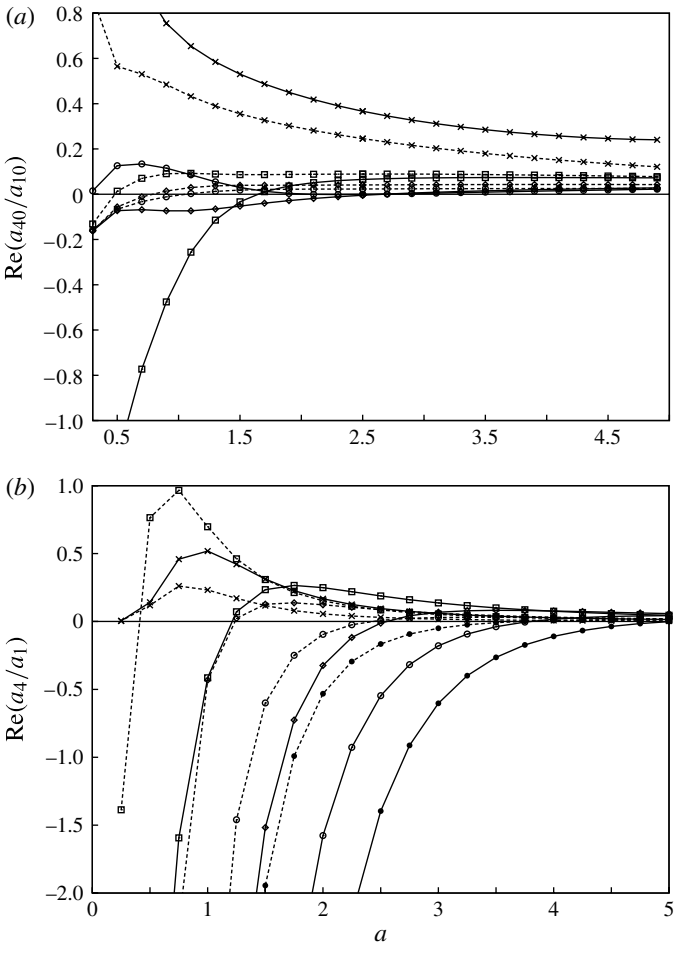

FIGURE 19. $\mathrm{Re}(a_4/a_1)$ as a function of local cone radius a for $a/r_s = 0.57$ and (*a*) $n = 0$; (*b*) $n = 1$. Results are shown using the regular microstructure model (2.5): —, $\phi_0 = \pi/4$; - - -, $\phi_0 = 0.2$. Symbols refer to mode number: ×, $m = 1$; □, $m = 2$; ◇, $m = 3$; ○, $m = 4$; ●, $m = 5$.

equation in their paper (cf. their equation (5.1)) with β_1, the leading-order scaled spanwise wavenumber. The results are shown for a scaled shock distance $\bar{y}_s = 1.73$ which corresponds to the shock angle expected from the flow conditions considered in this paper. Corresponding results shown in Seddougui & Bassom (1994) (cf. their figure 5) were obtained using incorrect values for two constants in their equation (4.12). Our corrected results shows the significant result that for a small range of $0 \leqslant \beta_1 \leqslant 0.7$, $\mathrm{Re}(a_3) > 0$. Thus nonlinear effects will be destabilizing for disturbances with these spanwise wavenumbers. By comparing the magnitudes of $\mathrm{Re}(a_3)$ and $\mathrm{Re}(a_4/a_1)$ we can infer that curvature has the effect of making the nonlinear effects stronger.

There have been some studies that investigate the nonlinear behaviour of viscous first-mode disturbances. Bicoherence diagrams from the experimental investigation of Bountin *et al.* (2010) show that in the low-frequency range ($f_1, f_2 < 100$ kHz) nonlinear processes proceed more intensely on the porous surface compared to the

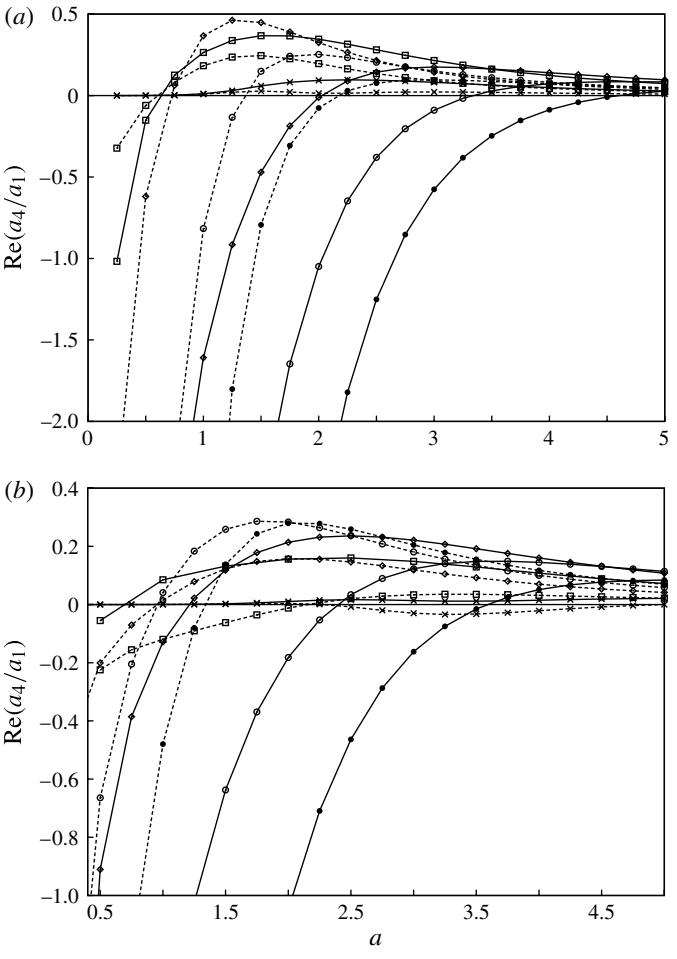

FIGURE 20. $\mathrm{Re}(a_4/a_1)$ as a function of local cone radius a for $a/r_s = 0.57$ and (*a*) $n = 2$; (*b*) $n = 3$. Results are shown using the regular microstructure model (2.5): —, $\phi_0 = \pi/4$; - - -, $\phi_0 = 0.2$. Symbols refer to mode number: ×, $m = 1$; □, $m = 2$; ◇, $m = 3$; ○, $m = 4$; ●, $m = 5$.

solid. The authors suggest that this may be caused by the growth of the low-frequency disturbance amplitudes due to surface roughness. Bicoherence measurements of Chokani *et al.* (2005) have also identified a nonlinear interaction that is associated with the destabilized Mack's first mode. Simulations by De Tullio & Sandham (2010) of transition over a flat plate in the presence of an oblique Mack's first mode show that the first mode grows faster than Mack's second mode and drives the flow directly to a turbulent state by nonlinear interactions. De Tullio & Sandham (2010) state that the first mode regains importance in the transition process at high Mach numbers for porous surfaces. Our results show that for sufficiently large a, nonlinear effects destabilize all linearly unstable viscous modes on a solid cone surface. At small values of a, corresponding to typical lengths of models tested in wind tunnels, it is the unstable mode with the lowest frequency that is destabilized by nonlinearity. Spatial instability results (Stephen & Michael 2012) indicate that these are the fastest growing disturbances but maximum growth rates are significantly smaller than the second

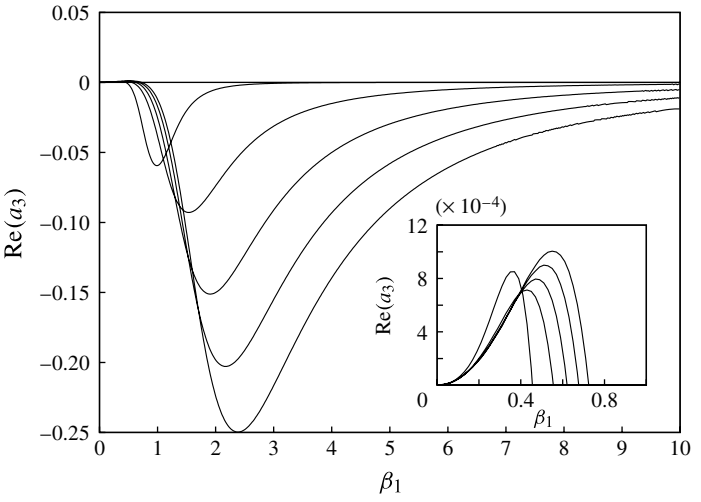

FIGURE 21. Re(a_3) for the first five modes as a function of spanwise wavenumber β_1 for $\bar{y}_s = 1.73$ (cf. equation (5.1) of Seddougui & Bassom 1994).

Mack mode. This may explain why in experiments transition has been observed due to the second Mack mode on solid cones. In the presence of porous walls, lower-frequency first Mack modes are also destabilized by nonlinearity while higher-frequency first Mack modes that are destabilized on the solid wall at a particular location now become stabilized for a range of a. This effect is enhanced by models with higher porosity. Thus over porous surfaces we can expect interaction of first Mack modes in the low-frequency spectrum to lead to nonlinear amplification of disturbance amplitudes beyond the critical value.

From this discussion it is clear that further research is required to establish whether Mack's first-mode instability can cause transition to turbulence in the presence of porous walls. The work presented here should be extended to consider resonant interactions between the unstable modes identified in this study and their harmonics. Parametric studies of porous-wall models are underway with the focus on minimizing the destabilizing effect on the first Mack mode (Wang & Zhong 2010, 2011*a*,*b*). Future stability and nonlinear interaction studies should include porous-wall models with these novel parameters and configurations. It is hoped that such studies will provide optimum design of porous coatings for incorporation into thermal protection systems as effective techniques for laminar flow control in hypersonic flight vehicles.

Acknowledgements

We are grateful to the referees for their careful comments which have led to the improvement of the presentation of the paper. This work was sponsored by the Air Force Office of Scientific Research, Air Force Material Command, USAF, under grant number FA8655-08-1-3044. The US Government is authorized to reproduce and distribute reprints for Governmental purpose notwithstanding any copyright notation thereon. V.M. acknowledges additional financial support from the School of Mathematics, University of Birmingham, UK.

Appendix

Definitions of the abbreviations *Tij*, *Lij* in equations (3.10) and (3.13):

$$T1 = \mathrm{i}^{-1/3} \int_{\xi_0}^{\infty} \left[K(\xi) + K'(\xi)(\xi - \xi_0)\right] \left(\int_{\xi_0}^{\xi} \mathrm{Ai}(s)\, \mathrm{d}s \right) \mathrm{d}\xi, \tag{A 1}$$

$$T3 = -\mathrm{i}^{-1/3} \mathrm{Ai}(\xi_0)\mathrm{Ai}'(\xi_0), \tag{A 2}$$

$$T6 = -\mathrm{i}^{1/3} \int_{\xi_0}^{\infty} K'(\xi) \left(\int_{\xi_0}^{\xi} \mathrm{Ai}(s)\mathrm{d}s \right) \left(\int_{\xi_0}^{\xi} \left(\int_{\infty}^{\xi_1} f^{**}(t)\, \mathrm{d}t \right) \mathrm{d}\xi_1 \right) \mathrm{d}\xi, \tag{A 3}$$

$$T7 = \mathrm{i}^{1/3} \left[\frac{\mathrm{d}H(\xi)}{\mathrm{d}\xi} \right]_{\xi=\xi_0}, \tag{A 4}$$

$$T8 = -\mathrm{i}^{4/3} \int_{\xi_0}^{\infty} K'(\xi) \left(\int_{\xi_0}^{\xi} H(t)\, \mathrm{d}t \right) \left(\int_{\xi_0}^{\xi} \mathrm{Ai}(s)\, \mathrm{d}s \right)^c \mathrm{d}\xi, \tag{A 5}$$

$$T10 = \mathrm{i}^{2/3} \int_{\xi_0}^{\infty} K'(\xi) \left(\int_{\xi_0}^{\xi} \left(\int_{\xi_0}^{t} H(s)\, \mathrm{d}s \right) \mathrm{d}t \right) \left(\mathrm{Ai}'(\xi)\right)^c \mathrm{d}\xi, \tag{A 6}$$

$$T11 = \mathrm{i}^{1/3} \int_{\xi_0}^{\infty} K'(\xi) \left(\int_{\xi_0}^{\xi} \left(\int_{\xi_0}^{t} \mathrm{Ai}(2^{1/3}s)\, \mathrm{d}s \right) \mathrm{d}t \right) (\mathrm{Ai}(\xi))^c \mathrm{d}\xi, \tag{A 7}$$

$$T12 = 2\mathrm{i}^{2/3} \int_{\xi_0}^{\infty} \bar{H}(t)\, \mathrm{d}t, \tag{A 8}$$

$$T13 = 2^{2/3}\mathrm{i}^{1/3} \int_{(2^{1/3}\xi)}^{\infty} \mathrm{Ai}(s)\, \mathrm{d}s, \tag{A 9}$$

$$T14 = -2^{1/3} \frac{\mathrm{d}}{\mathrm{d}\left(2^{1/3}\xi\right)} \left[\mathrm{Ai}\left(2^{1/3}\xi\right)\right]_{\xi=\xi_0}, \tag{A 10}$$

$$T15 = \mathrm{i}^{1/3} \int_{\xi_0}^{\infty} K'(\xi) \left(\mathrm{Ai}'(\xi) - \mathrm{Ai}'(\xi_0) - \xi \left(\int_{\xi_0}^{\xi} \mathrm{Ai}(s)\, \mathrm{d}s \right) \right) \left(\int_{\infty}^{\xi_1} f^{**}(t)\, \mathrm{d}t \right) \mathrm{d}\xi, \tag{A 11}$$

$$T16 = \int_{\xi_0}^{\infty} K'(\xi) \left(\mathrm{Ai}'(\xi) - \mathrm{Ai}'(\xi_0) - \xi \left(\int_{\xi_0}^{\xi} \mathrm{Ai}(s)\, \mathrm{d}s \right) \right)^c H(\xi)\, \mathrm{d}\xi, \tag{A 12}$$

$$T17 = \mathrm{i}^{-1/3} \int_{\xi_0}^{\infty} K'(\xi) \left(\mathrm{Ai}'(\xi) - \mathrm{Ai}'(\xi_0) - \xi \left(\int_{\xi_0}^{\xi} \mathrm{Ai}(s)\, \mathrm{d}s \right) \right)^c \mathrm{Ai}(2^{1/3}\xi)\, \mathrm{d}\xi, \tag{A 13}$$

$$T18 = \int_{\xi_0}^{\infty} K'(\xi) \left(\int_{\xi_0}^{\xi} \mathrm{Ai}(s)\, \mathrm{d}s \right) \mathrm{d}\xi, \tag{A 14}$$

$$T20 = T6 + T8 + 2T10 - T15 - T16, \tag{A 15}$$

$$T21 = T9 + 2T11 - T17, \tag{A 16}$$

$$T22 = \mathrm{i} \int_{\xi_0}^{\infty} K'(\xi) \left(\int_{\infty}^{\xi_1} f^{**}(t)\, \mathrm{d}t \right) \mathrm{Ai}'(\xi_0)\, \mathrm{d}\xi, \tag{A 17}$$

$$T23 = \int_{\xi_0}^{\infty} K'(\xi)\bar{H}(\xi)\mathrm{Ai}'\,(\xi_0)^c\, \mathrm{d}\xi, \tag{A 18}$$

$$T24 = \mathrm{i}^{-1/3} \int_{\xi_0}^{\infty} K'(\xi)\mathrm{Ai}(2^{1/3}\xi)\mathrm{Ai}'\,(\xi_0)^c\,\mathrm{d}\xi, \tag{A 19}$$

$$T25 = \mathrm{i} \int_{\xi_0}^{\infty} K'(\xi)\mathrm{Ai}\,(\xi)^c\,\mathrm{d}\xi, \tag{A 20}$$

$$L2 = -\mathrm{i}T1\kappa^{-1} - 2\mathrm{i}^{2/3}\mathrm{Ai}(\xi_0)\mathrm{Ai}'(\xi_0)\kappa^{-1}, \tag{A 21}$$

$$L9 = \left\{ 2\frac{\mathrm{i}n^2}{\alpha^{2/3}a^2} g_{2n}T13 - T14 + \left\{\alpha^{1/3} g_{2n}T13\right\} A_y \right\}^{-1}, \tag{A 22}$$

$$L10 = \left\{ T7 + 2\frac{\mathrm{i}n^2}{\alpha^{2/3}a^2} g_{2n}T12 + \left[\alpha^{1/3} g_{2n}T12 + T2\frac{g_n}{2}\right] A_y \right\}, \tag{A 23}$$

$$L11 = T20 - T21L9L10, \tag{A 24}$$

$$L12 = \alpha^{-4/3}T14L9L10 + \alpha^{-4/3}T7 - A_y\mathbb{P}_1T13, \tag{A 25}$$

$$L13 = T23 - T24L9L10, \tag{A 26}$$

$$L9^0 = \left\{ 2\mathrm{i}\alpha^{4/3} g^0_{2n}T13 - T14 + \left\{\alpha^{1/3} g^0_{2n}T13\right\} A_y \right\}^{-1}, \tag{A 27}$$

$$L10^0 = \left\{ T7 + 2\mathrm{i}\alpha^{4/3} g^0_{2n}T12 + \left[\alpha^{1/3} g^0_{2n}T12 + T2\frac{g^0_n}{2}\right] A_y \right\}, \tag{A 28}$$

$$L11^0 = T20 - T21L9^0L10^0, \tag{A 29}$$

$$L12^0 = \alpha^{-4/3}T14L9^0L10^0 + \alpha^{-4/3}T7 - A_y\mathbb{P}_{10}T13, \tag{A 30}$$

$$L13^0 = T23 - T24L9^0L10^0, \tag{A 31}$$

$$\mathbb{P}_{10} = \left(A_y + \mathrm{i}\alpha\right)^{-1}, \tag{A 32}$$

$$\mathbb{P}_{20} = \left(A_y + 2\mathrm{i}\alpha\right)^{-1}, \tag{A 33}$$

$$g_n = \frac{\mathrm{I}_n(\mathrm{i}\alpha r_s)\mathrm{K}_n(\mathrm{i}\alpha a) - \mathrm{I}_n(\mathrm{i}\alpha a)\mathrm{K}_n(\mathrm{i}\alpha r_s)}{\mathrm{I}_n(\mathrm{i}\alpha r_s)\mathrm{K}'_n(\mathrm{i}\alpha a) - \mathrm{I}'_n(\mathrm{i}\alpha a)\mathrm{K}_n(\mathrm{i}\alpha r_s)}, \tag{A 34}$$

$$g_{2n} = \frac{\mathrm{I}_{2n}(2\mathrm{i}\alpha r_s)\mathrm{K}_{2n}(2\mathrm{i}\alpha r) - \mathrm{I}_{2n}(2\mathrm{i}\alpha r)\mathrm{K}_{2n}(2\mathrm{i}\alpha r_s)}{\mathrm{I}'_{2n}(2\mathrm{i}\alpha a)\mathrm{K}_{2n}(2\mathrm{i}\alpha r_s) - \mathrm{I}_{2n}(2\mathrm{i}\alpha r_s)\mathrm{K}'_{2n}(2\mathrm{i}\alpha a)}, \tag{A 35}$$

$$g^0_n = \frac{\mathrm{I}_0(\mathrm{i}\alpha r_s)\mathrm{K}_0(\mathrm{i}\alpha r) - \mathrm{I}_0(\mathrm{i}\alpha r)\mathrm{K}_0(\mathrm{i}\alpha r_s)}{\mathrm{I}_0(\mathrm{i}\alpha r_s)\mathrm{K}'_0(\mathrm{i}\alpha a) - \mathrm{I}'_0(\mathrm{i}\alpha a)\mathrm{K}'_0(\mathrm{i}\alpha r_s)}, \tag{A 36}$$

$$g^0_{2n} = \frac{\mathrm{I}_0(2\mathrm{i}\alpha r_s)\mathrm{K}_0(2\mathrm{i}\alpha r) - \mathrm{I}_0(2\mathrm{i}\alpha r)\mathrm{K}_0(2\mathrm{i}\alpha r_s)}{\mathrm{I}_0(2\mathrm{i}\alpha r_s)\mathrm{K}'_0(2\mathrm{i}\alpha a) - \mathrm{I}'_0(2\mathrm{i}\alpha a)\mathrm{K}'_0(2\mathrm{i}\alpha r_s)}. \tag{A 37}$$

Functions $\bar{H}(\xi)$ and $f^{**}(\xi)$ are defined in Michael (2012).

REFERENCES

BASSOM, A. P. 1989 Weakly nonlinear lower-branch stability of fully developed and developing free-surface flows. *IMA J. Appl. Maths* **42**, 269–301.

BESTEK, H. & EISSLER, W. 1996 Direct numerical simulation of transition in Mach 4.8 boundary layers at flight conditions. In *Engineering Turbulence Modelling and Experiments* (ed. W. Rodi & G. Bergeles). vol. 3. Elsevier.

BOUNTIN, D., MASLOV, A., CHIMYTOV, C. & SHIPLYUK, A. 2010 Bispectral analysis of nonlinear processes in the hypersonic boundary layer on a porous cone surface. *Fluid Dyn.* **45**, 415–421.

BOUNTIN, D., SHIPLYUK, A. & MASLOV, A. 2008 Evolution of nonlinear processes in a hypersonic boundary layer on a sharp cone. *J. Fluid Mech.* **611**, 427–442.

BOUNTIN, D., SHIPLYUK, A. & SIDORENKO, A. 2000 Experimental investigations of disturbance development in the hypersonic boundary layer on conical models. In *Fifth IUTAM Symposium on Laminar–Turbulent Transition* (ed. H. F. Fasel & W. S. Saric). Springer.

BROWN, S. N., KHORRAMI, A. M., NEISH, A. & SMITH, F. T. 1991 On hypersonic boundary-layer interactions and transition. *Phil. Trans. R. Soc. Lond.* A **335**, 139–152.

CHANG, C.-L., MALIK, M. R. & HUSSAINI, M. Y. 1990 Effects of shock on the stability of hypersonic boundary layers. *AIAA Paper* 90-1448.

CHOKANI, N. 1999 Nonlinear spectral dynamics of hypersonic laminar boundary layer flow. *Phys. Fluids* **11**, 3846–3851.

CHOKANI, N. 2005 Nonlinear evolution of Mack modes in a hypersonic boundary layer. *Phys. Fluids* **17**, 014102.

CHOKANI, N., BOUNTIN, D. A., SHIPLYUK, A. N. & MASLOV, A. A. 2005 Nonlinear aspects of hypersonic boundary-layer stability on a porous surface. *AIAA J.* **43**, 149–155.

COWLEY, S. J. & HALL, P. 1990 On the instability of hypersonic flow past a wedge. *J. Fluid Mech.* **214**, 17–42.

DE TULLIO, N. & SANDHAM, N. D. 2010 Direct numerical simulation of breakdown to turbulence in a Mach 6 boundary layer over a porous surface. *Phys. Fluids* **22**, 094105–15.

DUCK, P. W. & HALL, P. 1989 On the interaction of Tollmien–Schlichting waves in axisymmetric supersonic flows. *Q. J. Mech. Appl. Maths* **42**, 115–130.

DUCK, P. W. & HALL, P. 1990 Non-axisymmetric viscous lower-branch modes in axisymmetric supersonic flows. *J. Fluid Mech.* **213**, 191–201.

EGOROV, I. V., FEDOROV, A. V. & SOUDAKOV, V. G. 2008 Receptivity of a hypersonic boundary layer over a flat plate with a porous coating. *J. Fluid Mech.* **601**, 165–187.

FEDOROV, A. V. 2011 Transition and stability of high-speed boundary layers. *Annu Rev. Fluid Mech.* **43**, 79–95.

FEDOROV, A., KOZLOV, V., SHIPLYUK, A., MASLOV, A. & MALMUTH, N. 2006 Stability of hypersonic boundary layer on porous wall with regular microstructure. *AIAA J.* **44**, 1866–1871.

FEDOROV, A. V., MALMUTH, N. D., RASHEED, A. & HORNUNG, H. G. 2001 Stabilization of hypersonic boundary layers by porous coatings. *AIAA J.* **39**, 605–610.

FEDOROV, A. V., SHIPLYUK, A., MASLOV, A. A., BUROV, E. & MALMUTH, N. D. 2003*a* Stabilization of high speed boundary layer using a porous coating. *AIAA Paper* 2003-1970.

FEDOROV, A. V., SHIPLYUK, A., MASLOV, A. A., BUROV, E. & MALMUTH, N. D. 2003*b* Stabilization of a hypersonic boundary layer using an ultrasonically absorptive coating. *J. Fluid Mech.* **479**, 99–124.

FEDOROV, A. & TUMIN, A. 2010 Branching of discrete modes in high-speed boundary layers and terminology issues. *AIAA Paper* 2010-5003.

GAPONOV, S., ERMOLAEV, Y., KOSINOV, A., LYSENKO, V., SEMENOV, N. & SMORODSKY, B. 2010 The influence of surface porosity on the stability and transition of supersonic boundary layer on a flat plate. *Thermophys. Aeromech.* **17**, 259–268.

GAPONOV, S. & TEREKHOVA, N. M. 2009 Three-wave interactions between disturbances in the hypersonic boundary layer on impermeable and porous surfaces. *Fluid Dyn.* **44**, 362–371.

GERMAIN, P. D. & HORNUNG, H. G. 1997 Transition on a slender cone in hypervelocity flow. *Exp. Fluids* **22** (3), 183–190.

HALL, P. & SMITH, F. T. 1982 A suggested mechanism for nonlinear wall roughness effects on high Reynolds number flow stability. *Stud. Appl. Maths* **66**, 241–265.

HALL, P. & SMITH, F. T. 1984 On the effects of nonparallelism, three-dimensionality, and mode interaction in nonlinear boundary-layer stability. *Stud. Appl. Maths* **70**, 91–120.

HAYES, W. D. & PROBSTEIN, R. F. 1966 *Hypersonic Flow Theory*, 2nd edn., vol. 1. Academic.

HUSMEIER, F. & FASEL, H. F. 2007 Numerical investigations of hypersonic boundary layer transition for circular cones. *AIAA Paper* 2007-3843.

KIMMEL, R. 2003 Aspects of hypersonic boundary layer transition control. *AIAA Paper* 2003-0772.

KIMMEL, R. L., DEMETRIADES, A. & DONALDSON, J. C. 1996 Space–time correlation measurements in a hypersonic transitional boundary layer. *AIAA J.* **34**, 2484–2489.

KIMMEL, R. L. & KENDALL, J. M. 1991 Nonlinear disturbance in a hypersonic boundary layer. *AIAA Paper* 91-0320.

KLUWICK, A., GITTLER, P. & BODONYI, R. J. 1984 Viscous-inviscid interactions on axisymmetric bodies of revolution in supersonic flow. *J. Fluid Mech.* **140**, 280–301.

KOEVARY, C., LAIBLE, A., MAYER, C. & FASEL, H. F. 2010 Numerical simulations of controlled transition for a sharp circular cone at Mach 8. *AIAA Paper* 2010-4598.

KOZLOV, V. F., FEDOROV, A. & MALMUTH, N. 2005 Acoustic properties of rarefied gases inside pores of simple geometries. *J. Acoust. Soc. Am.* **117**, 3402–3412.

LACHOWICZ, J. T., CHOKANI, N. & WILKINSON, S. P. 1996 Boundary-layer stability measurements in a hypersonic quiet tunnel. *AIAA J.* **34** (12), 2496–2500.

LAIBLE, A. & FASEL, H. F. 2011 Numerical investigation of hypersonic transition for a flared and a straight cone at Mach 6. *AIAA Paper* 2011-3565.

LEUNG, K. K. & EMANUEL, G. 1995 Hypersonic inviscid and viscous flow over a wedge and cone. *J. Aircraft* **32**, 385–391.

LUKASHEVICH, S. V., MASLOV, A. A., SHIPLYUK, A. N., FEDOROV, A. V. & SOUDAKOV, V. G. 2010 Stabilization of high-speed boundary layer using porous coatings of various thicknesses. *AIAA Paper* 2010-4720.

MACK, L. M. 1984 Boundary layer stability theory. In *Special Course on Stability and Transition of Laminar Flow*, *AGARD Rep.* 709.

MALIK, M. R. 1990 Numerical-methods for hypersonic boundary-layer stability. *J. Comput. Phys.* **86**, 376–413.

MASLOV, A. 2003 Experimental and theoretical studies of hypersonic laminar flow control using ultrasonically absorptive coatings (U.A.C.). *Tech. Rep.* ISTC 2172-2001. International Science and Technology Centre.

MASLOV, A. A., POPLAVSKAYA, T. & BOUNTIN, D. A. 2010 Hypersonic boundary layer transition and control. In *Seventh IUTAM Symposium on Laminar–Turbulent Transition* (ed. P. Schlatter & D. Henningson). pp. 19–26. Springer.

MICHAEL, V. 2012 Effects of passive porous walls on the first Mack mode instability of hypersonic boundary layers over a sharp cone. PhD thesis, University of Birmingham..

NEILAND, V. Y. 1969 Theory of laminar boundary layer separation in supersonic flow. *Izv. Akad. Nauk. SSSR Mech. Zhidk Gaza* 53–57.

PRUETT, C. D. & CHANG, C.-L. 1995 Spatial direct numerical simulation of high speed boundary-layer flows. Part II: transition on a cone in Mach 8 flow. *Theoret. Comput. Fluid Dyn* **7**, 397–424.

RASMUSSEN, M. 1994 *Hypersonic Flow*. Wiley.

REED, H. L., KIMMEL, R., SCHNEIDER, S., ARNAL, D. & SARIC, W. 1997 Drag prediction and transition in hypersonic flow. *AIAA Paper* 97-1818.

SCHNEIDER, S. P. 2004 Hypersonic laminar-turbulent transition on circular cones and scramjet forebodies. *Prog. Aerosp. Sci.* **40** (1-2), 1–50.

SEDDOUGUI, S. O. 1994 Stability of hypersonic flow over a cone. In *Transition, Turbulence and Combustion* (ed. M. Y. Hussaini, T. B. Gatski & T. L. Jackson). pp. 50–59. Kluwer.

SEDDOUGUI, S. O. & BASSOM, A. P. 1994 Nonlinear instability of viscous modes in hypersonic flow past a wedge. *Q. J. Mech. App. Maths* **47**, 557–582.

SEDDOUGUI, S. O. & BASSOM, A. P. 1997 Instability of hypersonic flow over a cone. *J. Fluid Mech.* **345**, 383–411.

SHIPLYUK, A. N., BOUNTIN, D. A., MASLOV, A. A. & CHOKANI, N. 2003 Nonlinear mechanisms of the initial stage of the laminar–turbulent transition at hypersonic velocities. *J. Appl. Mech. Tech. Phy.* **44**, 654–659.

SMITH, F. T. 1979 Nonlinear stability of boundary layers for disturbances of various sizes. *Proc. R. Soc. Lond.* A **368**, 573–589.

SMITH, F. T. 1980 Corrections to 'Nonlinear stability of boundary layers for disturbances of various sizes'. *Proc. R. Soc. Lond.* A **371**, 439–440.

SMITH, F. T. 1989 On the first-mode instability in subsonic, supersonic or hypersonic boundary layers. *J. Fluid Mech.* **198**, 127–153.

STEPHEN, S. O. 2006 Nonlinear instability of hypersonic flow over a cone. *Q. J. Mech. App. Maths* **59**, 301–319.

STEPHEN, S. O. & MICHAEL, V. 2010*a* Effect of passive porous walls on hypersonic boundary layer. In *Seventh IUTAM Symposium on Laminar-Turbulent Transition* (ed. P. Schlatter & D. Henningson). pp. 581–584. Springer.

STEPHEN, S. O. & MICHAEL, V. 2010*b* Effects of porous walls on hypersonic boundary layer over a sharp cone. *AIAA Paper* 2010-4286.

STEPHEN, S. O. & MICHAEL, V. 2012 Effects of porous walls on hypersonic boundary layers over a sharp cone. School of Mathematics Preprint Series 2012/06, University of Birmingham.

STETSON, K. F. 1988 On nonlinear aspects of hypersonic boundary-layer stability. *AIAA J.* **26** (7), 883–885.

STETSON, K. & KIMMEL, R. 1992 On hypersonic boundary-layer stability. *AIAA Paper* 92-0737.

STETSON, K. F., KIMMEL, R., THOMPSON, E. R., DONALDSON, J. C. & SILER, L. G. 1991 A comparison of planar and conical boundary layer stability and transition at a Mach number of 8. *AIAA Paper* 91-1639.

STETSON, K. F., THOMPSON, E. R., DONALDSON, J. C. & SILER, L. G. 1983 Laminar boundary layer-stability experiments on a cone at Mach 8. Part 1: sharp cone. *AIAA Paper* 83-1761.

STEWARTSON, K. 1964 *The Theory of Laminar Boundary Layers in Compressible Fluids*. Oxford University Press.

STEWARTSON, K. & WILLIAMS, P. G. 1969 Self-induced separation. *Proc. R. Soc. Lond.* A **312**, 181–206.

STILLA, J. 1994 Engineering transition prediction for a hypersonic axisymmetric boundary layer. *J. Aircraft* **31**, 1358–1364.

STUART, J. T. 1960 On the nonlinear mechanics of wave disturbances in stable and unstable parallel flows. *J. Fluid Mech.* **9**, 353–370.

STUCKERT, G. & REED, H. L. 1994 Linear disturbances in hypersonic, chemically reacting shock layers. *AIAA J.* **32**, 1384–1393.

TAYLOR, G. & MACCOLL, J. 1933 The air pressure on a cone moving at high speeds.- I. *Proc. R. Soc. Lond.* A **139**, 278–297.

WANG, X. & ZHONG, X. 2009 Numerical simulation and theoretical analysis on boundary-layer instability affected by porous coating. *AIAA Paper* 2009-3679.

WANG, X. & ZHONG, X. 2010 Effect of porous coating on boundary-layer instability. *AIAA Paper* 2010-1243.

WANG, X. & ZHONG, X. 2011*a* Phase angle of porous coating admittance and its effect on boundary-layer stabilization. *AIAA Paper* 2011-3080.

WANG, X. & ZHONG, X. 2011*b* Numerical simulations on mode S growth over feltmetal and regular porous coatings of a Mach 5.92 flow. *AIAA Paper* 2011-375.

WHITEHEAD, A. JR. 1989 NASP aerodynamics. *AIAA Paper* 89-5013.

ZHONG, X. & WANG, X. 2012 Direct numerical simulation on the receptivity, instability, and transition of hypersonic boundary layers. *Annu. Rev. Fluid Mech.* **44**, 527–561.